SF 298 MASTER COPY KEEP THIS COPY FOR REPRODUCTION PURPOSES

REPORT DOCUMENTATION PAGE

Form Approved
OMB NO. 0704-0188

1. AGENCY USE ONLY *(Leave blank)*	2. REPORT DATE	3. REPORT TYPE AND DATES COVERED
	12/30/96	Final 1/20/93 - 9/30/96

4. TITLE AND SUBTITLE
Ultra-High Bandwidth Tunneling Injection Lasers

5. FUNDING NUMBERS
DAAH04-93-G-0034

6. AUTHOR(S)
Pallab Bhattacharya

7. PERFORMING ORGANIZATION NAMES(S) AND ADDRESS(ES)
University of Michigan
Department of Electrical Engineering & Computer Science
1301 Beal Avenue
Ann Arbor, MI 48109-2122

8. PERFORMING ORGANIZATION REPORT NUMBER

9. SPONSORING / MONITORING AGENCY NAME(S) AND ADDRESS(ES)
U.S. Army Research Office
P.O. Box 12211
Research Triangle Park, NC 27709-2211

10. SPONSORING / MONITORING AGENCY REPORT NUMBER
ARO 31008.3-EL-SDI

11. SUPPLEMENTARY NOTES
The views, opinions and/or findings contained in this report are those of the author(s) and should not be construed as an official Department of the Army position, policy or decision, unless so designated by other documentation.

12a. DISTRIBUTION / AVAILABILITY STATEMENT
Approved for public release; distribution unlimited.

12 b. DISTRIBUTION CODE

13. ABSTRACT *(Maximum 200 words)*

In conventional quantum well lasers, carriers are injected into the quantum wells with quite high energies. We have invented a new quantum well laser in which electrons are injected into the quantum well ground state through tunneling. The *tunneling injection lasers* are shown to have negligible gain compression, superior high temperature performance, lower Auger recombination and wavelength chirp, and better modulation characteristics when compared to conventional lasers. The underlying physical principles behind the superior performance are also explored and calculations and measurements of relaxation times in quantum wells have been made. Experimental results have been obtained for lasers made with a variety of material systems, InGaAs/GaAs/AlGaAs, InGaAs/GaAs/InGaAsP, and InGaAs/InGaAsP/InP, for different applications. Both single quantum well and multiple quantum well tunneling injection lasers are demonstrated. These lasers outperform any other semiconductor laser in terms of modulation bandwidth and gain compression. $f_{-3dB} \sim 50$ GHz and $f_{-3dB}(max)=98$ GHz have been measured. This device is now being investigated on a worldwide basis, and the tunneling mechanism has also been incorporated in VCSELs.

14. SUBJECT TERMS	15. NUMBER IF PAGES
Tunneling and High-Speed Lasers	58
	16. PRICE CODE

17. SECURITY CLASSIFICATION OR REPORT	18. SECURITY CLASSIFICATION OF THIS PAGE	19. SECURITY CLASSIFICATION OF ABSTRACT	20. LIMITATION OF ABSTRACT
UNCLASSIFIED	UNCLASSIFIED	UNCLASSIFIED	UL

Final Technical Report

Title: Ultra-High Bandwidth Tunneling Injection Lasers

Grant No. DAAH04-93-G-0034

P.I.: P. Bhattacharya
Solid State Electronics Laboratory
Department of Electrical Engineering & Computer Science
The University of Michigan
Ann Arbor, Michigan 48109-2122
Phone: (313) 763-6678 Fax: (313) 763-9324 e-mail: pkb@eecs.umich.edu

Period Covered: 1/20/93 - 9/30/96

FORWARD

In conventional quantum well lasers, carriers are injected into the quantum wells with quite high energies. We have invented a new quantum well laser in which electrons are injected into the quantum well ground state through tunneling. The *tunneling injection lasers* are shown to have negligible gain compression, superior high temperature performance, lower Auger recombination and wavelength chirp, and better modulation characteristics when compared to conventional lasers. The underlying physical principles behind the superior performance are also explored and calculations and measurements of relaxation times in quantum wells have been made. Experimental results have been obtained for lasers made with a variety of material systems, InGaAs/GaAs/AlGaAs, InGaAs/GaAs/InGaAsP, and InGaAs/InGaAsP/InP, for different applications. Both single quantum well and multiple quantum well tunneling injection lasers are demonstrated. These lasers outperform any other semiconductor laser in terms of modulation bandwidth and gain compression. $f_{\text{-3dB}} \sim 50$ GHz and $f_{\text{-3dB}}(\text{max})=98$ GHz have been measured. This device is now being investigated on a worldwide basis, and the tunneling mechanism has also been incorporated in VCSELs.

TABLE OF CONTENTS

List of Illustrations

1. INTRODUCTION

Over the last decade quantum well lasers have become ubiquitous in the area of optical communications [1]. The quasi-2-dimensional world provided by the quantum wells allows modification of the carrier density of states leading to lower threshold current density. As a result, lattice matched and strained quantum well lasers can now be fabricated with sub-milliamp threshold current [2]. Recently, however, some attention has been focussed on potentially negative aspects of sub-3-dimensional systems. These negative aspects have bearing on the high speed performance of the lasers as well as the temperature dependence of the threshold current. The aspects under discussion arise from the carrier thermalization times in sub-3-dimensional systems [3], carrier loss due to injection over the barriers in quantum well lasers [4], and the related issues of carrier distribution being at non-quasi-equilibrium resulting in non-linear gain and hot carrier effects [5].

To understand the issues raised above we show in Fig. 1 the carrier injection process in a conventional separate confinement heterostructure (SCH) quantum well lasers. Electrons and holes are injected from the cladding layer regions into the quantum well. Since the cladding layers are made from larger bandgap materials (this region must have a smaller refractive index), the carriers are injected into the active region with energies of the order of several hundred millielectron volts. *For efficient laser performance the carriers should be able to enter the quantum well and reach thermal equilibrium with the quasi-Fermi level.* This requires the carriers to emit phonons (optical phonons) at a very rapid rate, and also avoid being swept over the barrier into the opposite cladding layer as shown in Fig. 1. Carriers that cross the active region are lost as far as lasing is concerned and are a significant source of poor temperature performance of lasers. If carriers entering the quantum well region do not thermalize, the carrier distribution will become hot, resulting in two negative effects. The hot carrier distribution will provide lower gain at the lasing energy which arises from the ground states of the quantum well. Also, the Auger recombination will

be enhanced. These effects will become of greater importance as the laser is pumped harder to achieve higher modulation bandwidths. As the laser is pumped harder, the electron-hole recombination time determined by stimulated emission becomes very short (as small as 20 ps). If injected carriers cannot lose energy and thermalize in these times, the carrier distribution will become even hotter. This leads to non-linear gain and increased Auger recombination.

In view of the importance of the carrier thermalization times, it is useful to review these times in bulk and quantum confined systems. We will focus on the electron relaxation since the hole relaxation is very fast due to the high scattering rates for holes. It has been shown that electron thermalization times are of the order of one picosecond in bulk direct gap semiconductors. For quantum wells the times increase to $\sim 5 - 15$ ps depending upon the well size and the carrier density [6]. In quantum wires the times can be as long as 30 ps [7]. One can see that quantum systems which offer superior density of states for low threshold lasing suffer from long relaxation times.

Recently, we have been developing a new approach for carrier injection in quantum well lasers to bypass the carrier thermalization problem and yet exploit the two-dimensional density of states. The approach is based on the injection of electrons into the quantum well by tunneling through a resonant tunneling barrier [8]. The approach shown schematically in Fig. 2 is based on the following two steps: i) electrons coming from the cladding layer are first thermalized in a wide (3-dimensional) region before reaching the quantum well; ii) the thermalized "cold" electrons now enter the quantum well region through the resonant tunneling barrier as shown in Fig. 2. The injection of holes is done in a manner similar to that in conventional lasers. This is because as noted above there is no problem in hole thermalization process in quantum wells. The approach outlined above has several expected benefits which we outline here:

i) Since electrons are injected into the quantum well as "cold" electrons the electron gas does not suffer from hot carrier effects discussed earlier;

ii) The injection mechanism also ensures that very few electrons will go over the active region into the opposite cladding layer;

iii) Gain compression effects will be minimized since the majority of electrons are injected close to the lasing energy.

iv) Since the tunneling process produces an initial carrier distribution which has an energy spread much smaller than the thermal energy kT at room temperature, it is possible that the spectral purity will improve. Also the Auger recombination may be reduced for such a sharp electron distribution. Of course, even if the electrons are injected with a very narrow energy spread, the electron distribution will broaden from scattering once the electrons are in the quantum well.

2. BASIS FOR THE TUNNELING LASER: CARRIER CAPTURE AND RELAXATION IN NARROW QUANTUM WELLS

It has been recognized that the intrinsic limit on the modulation frequency of a semiconductor laser is strongly dependent on the carrier relaxation process [6, 9]. In studying such effects, not only should diffusion effects [10] be included, but it is equally important to consider quantum capture times and the scattering effects in the confinement layer. Such a study undertaken by us is described in this section.

In our theoretical study, for which a Monte Carlo approach was adopted, it was assumed that the relaxation processes in the conduction band will be much slower than those in the valence band, and will therefore dominate the device response [3, 11, 12]. Furthermore, because of the nonparabolicities and band-mixing effects in the valence band structure, a study of the relaxation process in the conduction band is a better starting point for a theoretical analysis of carrier equilibration. Hence, only electron transport is considered. The procedure for our calculations is briefly outlined. The eigenfunctions for electrons in the confined system are calculated from which the bulk and confined states are obtained. The appropriate scattering processes in the subband of the quantum well are calculated. In our Monte Carlo method, a

charge distribution is injected in the 3D region (inner cladding layer) with a thermal distribution and the temporal response of the injected charge is observed. The carrier transport in the 3D SCH region and the 2D well region are modeled separately. During carrier relaxation in the quasi-two-dimensional environment of the quantum well, the carriers experience both intrasubband and intersubband scattering with the lattice vibrations. For the case of an unintentionally doped well region at low carrier concentrations, the dominant scattering mechanisms are polar optical phonon and acoustic phonon scattering. Using the Fermi Golden Rule, the intersubband optical phonon scattering rates are given by [13, 14]

$$S_{mn}^{POP} = \frac{e^2\omega_o}{8\pi\epsilon_o}\left[\frac{1}{\epsilon_\infty} - \frac{1}{\epsilon_s}\right]\left(N_q + \frac{1}{2} \mp \frac{1}{2}\right)\int \frac{H_{mn}(Q)Q}{Q^2+Q_o^2}\delta(E(\mathbf{k_2}) - E(\mathbf{k_1}) \pm \hbar\omega_o)d\mathbf{k_2} \quad (1)$$

where the Bose-Einstein distribution gives the phonon occupation number

$$N_q = \frac{1}{exp\left(\frac{\hbar\omega_o}{k_BT}\right) - 1}. \quad (2)$$

Here, $\hbar\omega$ is the polar optical phonon energy, taken as 35.36 meV, and $\epsilon_\infty = 10.92$ and $\epsilon_s = 12.90$ are the optical and static dielectric constants, respectively. The initial and final-state wavevectors of the electron are $\mathbf{k_1}$ and $\mathbf{k_2}$, while $Q = \pm(\mathbf{k_1} - \mathbf{k_2})$ and q are the phonon wavevector components parallel and perpendicular to the well layer. For simplicity, carrier screening effects [15] are included in (1) with $Q_o^2 = \epsilon^2 n/\epsilon k_B T$ as the Debye screening wavevector. $H_{mn}(Q)$ are the multisubband coupling coefficients. Calculation of the values of $H_{mn}(Q)$ in a quantum well by us [16] has clearly indicated that transitions between discrete electron levels in a quantum confined system are more difficult than in a bulk semiconductor due to the energy and momentum conservation requirements.

For our model, the polar optical phonon absorption scattering rate is also calculated and found to be about four times lower than the optical phonon emission rate. For completeness, we have calculated the acoustic phonon scattering rates as in Refs. 13 and 14, although it is about 100 times smaller than the optical phonon rates.

Electron-electron interactions become significant when the carrier density is moderately high ($n > 10^{17}$ cm^{-3}) [17]. The total screened electron-electron scattering rates for the 3D region are found using the Fermi Golden Rule [18, 19]. For the 2D region, the total electron-electron scattering rates are derived by summing over all final states the transition probability of two electrons in subbands i and j scattering into subbands m and n, respectively, after a collision [20]. Only dominant scattering processes are considered, which are pure intrasubband scattering where $i = m, j = n$, and $i \neq j$. We have implemented the 2D and 3D electron-electron scattering mechanisms in our model using a rejection method [21].

Figure 3(a) shows the temporal variation of the ground state occupancy when an ensemble of carriers are injected at an energy 0.15 eV above the quantum well in an SCH structure. Figure 3(b) depicts similar data for carriers injected into a linearly graded refractive index SCH (L-GRINSCH) structure. Again multiple injection densities have been chosen to simulate true injection conditions in a laser. Experimentally similar capture times have been measured by us and others [3, 16, 22] using time-resolved photoluminescence measurements and pump-probe techniques. It is therefore amply evident that the electron relaxation time to the ground state in quantum wells can be as high as 20 ps, depending on size. As stated earlier, the primary reason for this is that transitions between discrete levels in a quantum confined system are more difficult than in bulk semiconductors due to the energy and momentum conservation requirements.

Since the thermalization time can become longer than the stimulated emission time, for large injection currents the carrier distribution will no longer remain quasi-Fermi and instead becomes a hot carrier distribution. In fact, in a laser operated beyond threshold, the carrier temperature can be $\sim 40°$ higher than the lattice temperature.

3. THE TUNNELING CONCEPT AND ITS BENEFITS

If "cold" electrons are introduced into the lasing subband of the active quantum

well at or near the Fermi level by tunneling, as shown in Fig. 2, then the hot carrier effects discussed in the previous section are minimized. Electrons are injected at energies close to the lasing energy at a rate faster than the stimulated emission rate and the electron distribution remains quasi-Fermi even at large drive currents. By using a time-resolved pump-probe technique, we have measured the tunneling time to be $1 - 2$ ps in a laser structure identical to that shown in Fig. 2 [22]. Lutz *et al* [23] have also verified the tunneling mechanism in a tunneling injection laser by observing the expected hysteresis in both the current-voltage and the light-current characteristics of a GaAs-based tunneling injection (TI) laser.

Figure 4(a) shows the heterostructure of an GaAs-based TI laser designed for emission at 0.98 μm and Fig. 4(b) shows the design of a 1.55 μm InP-based laser. The structures were grown by molecular beam epitaxy (MBE) and metal-organic vapor phase epitaxy (MOVPE), respectively. The optical mode profile of the 1.55 μm laser of Fig. 4(b) is shown in Fig. 5. It is evident that there is very little asymmetry introduced due to the small perturbation of the active region and this is important for high-performance devices.

Broad-area and single-mode lasers are made with the same processing techniques as for SCH lasers. The standard photolithograhy and lift-off techniques followed by wet and dry chemical etching are used. Regrowth is used for buried-heterostructure index-guided devices. Ridge waveguide lasers are fabricated with a 3 μm wide stripe in a coplanar ground-signal-ground contact geometry, suitable for on-wafer microwave measurements.

It is generally believed that spectral hole burning and carrier heating are the two main causes of gain suppression in lasers. We have studied gain-compression effects in a GaAs-based tunneling injection laser by observing the spontaneous emission spectra during lasing as a function of bias current. A broad-area laser, 125 μm wide and 400 μm long is specially made with a window in the top p-ohmic contact through which the spontaneous emission exits. The laser is driven at different injection levels

and the spontaneous emission is collected and analyzed by a 0.75 m SPEX scanning spectrometer. The emerging light is detected with a Ge detector. The experimental arrangement is schematically shown in Fig. 6(a) and the measured data are shown in Fig. 6(b). The intensity of the spontaneous emission increases continuously at the lasing wavelength with increase of injection current, indicating absence of gain compression at the lasing wavelength. The oscillations observed in the spectra are due to spurious Fabry-Perot resonances, possibly between the n-side electrode and the various layers of the heterostructures. If gain compression effects are severe, then little or no increase in the spontaneous emission intensity would be expected at the lasing wavelength, as recently reported by Girardin *et al* [24] for a 1.5 μm laser. The relative contributions of spectral hole burning and carrier heating in a semiconductor laser are strongly dependent on the laser type and material in the active region [25-28]. Theoretical studies indicate that strained quantum well lasers exhibit enhanced carrier heating effects due to the extremely low threshold carrier density [5]. Carrier heating effects are manifested in the spontaneous emission spectra as a gain suppression at wavelengths *below* the gain maximum and closer to the peak of the spontaneous emission spectrum [24, 29]. Although the device used in this study is a $In_{0.2}Ga_{0.8}As/GaAs$ strained quantum well laser, it has only one lasing well and I_{th} is quite high. Therefore, n_{th} is expected to be high. It is difficult, therefore, to distinguish spectral hole burning and carrier heating effects and it is probably accurate to state that both effects contribute to a reduction of gain compression in the TI laser in an indistinguishable manner.

4. MODULATION BANDWIDTH AND DYNAMIC LINEWIDTH (CHIRP) OF SQW TUNNELING INJECTION LASERS

It is well recognized [1] that gain suppression is one of the most limiting effects in the dynamic behavior of a laser, in particular the modulation bandwidth and

wavelength chirp of directly modulated lasers. The reduction of gain compression achieved in the tunneling injection lasers promise higher bandwidth and lower chirp. At the same time it is expected that the temperature dependence of J_{th} will be reduced. We have verified these in ~ 0.98 μm lasers.

Measurements were made on a $3\mu m \times 200\mu m$ ridge waveguide laser grown by MBE and fabricated on semi-insulating GaAs substrate [30]. The facets are uncoated. From the measured L-I characteristics the values of I_{th}, cavity loss, slope efficiency and internal quantum efficiency are obtained to be $3-4$ mA, 13 cm^{-1}, 0.31 mW/mA per facet, and 0.56, respectively. The differential gain of these devices varied in the range $(5-6) \times 10^{-16}$ cm^2, which is a factor of 2 higher than the best value for a SQW-SCH laser [31] and comparable to the best MQW-SCH devices, even with 35% In in the active wells (remember that our devices have 20% In). The internal modulation bandwidth of the lasers were measured with help of a sweep oscillator, a New Focus high-speed (40 GHz) detector and a HP spectrum analyzer. The devices were placed on Cu heatsinks without using In and were not bonded to carriers. High-frequency probes and a bias-T were used to access the devices on wafer and to provide the DC bias, together with the microwave input. The modulation response data are shown in Fig. 7 for an output power of 15 mW. The -3 dB bandwidth is 12.5 GHz, which is higher than any value obtained for a SQW-SCH ridge waveguide device.

The temperature dependence of the threshold current was measured in the range $298-343$ K. By fitting the data with the phenomenological expression, $I_{th} = I_o exp(T/T_o)$, an average T_o of 170 K is obtained for several devices. A very high value of 219 K was obtained in one device. These values are considerably higher than those in SCH devices, where T_o is usually ~ 125 K.

We have measured the dynamic linewidth (wavelength chirp) of a GaAs-based 0.91 μm TI laser and have compared them with SCH and DFB lasers emitting at 1.07 and 1.3 μm respectively. The cavity lengths and threshold currents of the SCH, TI and DFB lasers are 300, 350 and 400 μm, and 11.8, 11.5 and 11.3 mA, respectively. Chirp

was measured up to modulation frequencies of 20 GHz at a fixed value of bias current (20 mA) and peak-to-peak modulation current (14 mA). The chirp was estimated to be the full width at half maximum of the dominant lasing longitudinal mode measured by a low-speed photodiode from a 0.75 m scanning spectrometer. The Fabry-Perot mode shifting due to device heating was minimized by using a pulsed bias (1 μm pulse width and 5 KHz repetition rate). The measured dynamic linewidth of the three lasers are shown in Fig. 8. Two characteristics are immediately evident. First, the measured linewidths are not sensitive to the modulation frequency ω_m, as expected, in this frequency range. This observation has been made by other authors [32]. Second, the chirp in the TI laser is lower than that in the SCH laser, and almost comparable to that of the DFB laser, whose dynamic linewidths are characteristically low due to the mode pulling mechanism. We attribute this significant reduction of chirp in the TI laser to the reduction of hot carriers and the gain compression factor ϵ [33].

5. InP-BASED 1.55μm TUNNELING INJECTION LASERS

Auger recombination, which is a three-carrier non-radiative recombination process, is one of the more serious drawbacks of long wavelength InGaAsP/InP lasers. The presence of hot carriers enhances the rate of the conduction-heavy hole-heavy hole-split off band (CHHS) Auger process, given by $R_{Auger} = C_a np^2$, where C_a is the Auger coefficient. We have made extensive measurements of the Auger recombination coefficients in the TI lasers and compared them with 1.55 μm MQW-SCH lasers [34]. A typical InP-based TI laser heterostructure was shown in Fig. 4(b). The details of the measurements and analysis of data are not repeated here, but only the final results. Measurements were made for several cavity lengths in each laser. Compared to an average value of $C_a = 1 \times 10^{-27}$ cm^6/s for the SCH devices (averaged over the cavity lengths), an average value of $C_a = 8 \times 10^{-31}$ cm^6/s was obtained for the

TI lasers. *This represents a reduction of over 3 orders of magnitude in the value of* C_a. Furthermore, considering the fact that Auger recombination in MQW lasers is generally smaller than in SQW devices, due to a lower hot carrier density in the former, this result is all the more significant.

Typical measured temperature-dependent variation of the L-I characteristics of these lasers in the range $283-338$ K are depicted in Fig. 9. From such measurements an average value of $T_o = 54$ K and a high value of $T_o = 70$ K are derived. Even the average value is ~ 1.5 times typical values of T_o obtained in 1.55 μm MQW-SCH lasers. Recently Fukushima *et al* [35] have measured a value of $T_o = 50-60$ K in a 1.55 μm laser in which a MQW barrier is introduced in the inner cladding layer. The effect of this barrier is to prevent carriers from escaping the MQW region and optimize carrier capture. Zah *et al* [36] have measured $T_o = 82$ K by incorporating higher energy barriers in the MQW to prevent carrier leakage and improve confinement. It must be remembered that several factors contribute to low T_o. These are hot carriers, carrier leakage, intervalence band absorption and heterointerface recombination. In the TI laser, with the present design, the hot carrier population is minimized. We believe that with more optimal design, T_o can be enhanced further.

6. OTHER MATERIAL SYSTEMS

The use of $In_{0.49}Ga_{0.51}P$ lattice matched to GaAs (hereafter referred to as InGaP) with a bandgap of ~ 1.89 eV as the cladding layer of InGaAs/GaAs 0.98 μm lasers is becoming increasingly prevalent for high power pump lasers in optical communication. The use of this material provides several advantages. It has better thermal conductivity than the typical $Al_{0.4}Ga_{0.6}As$ used in GaAs-based lasers [37]. The GaAs/InGaP heterointerface has an extremely low interface recombination velocity of 1.5 cm/s [38]. The gradual degradation of InGaAs/GaAs/AlGaAs lasers, generally attributed to Al oxidation induced facet degradation, will be eliminated and will make these lasers suitable for reliable high-power operation. The existence of reliable selective

etchant between GaAs and InGaP makes the fabrication of stripe geometry lasers simpler. However, there may be a couple of disadvantages. The large index difference between GaAs and InGaP can cause wide transverse beam divergence. Also, in spite of $\Delta E_c < \Delta E_v$ [39, 40] for the GaAs/InGaP heterojunction, the value of ΔE_c is still ~ 0.2 eV, which may inhibit carrier injection across an abrupt heterointerface. The use of graded InGaAsP layers, or the tunneling injection structure will alleviate this problem.

In view of what has been stated above, we have made and characterized the first InGaAs/GaAs/InGaP TI lasers. The SQW-TI heterostructure grown by MOVPE on semi-insulating GaAs substrates oriented 5° off (001) toward [110] is shown in Fig. 10. It is useful to note that InGaAsP quaternary layer ($E_g = 1.6$ eV) lattice matched to GaAs on the p-side of the active region helps in the efficient injection of holes from the p-contact. The tunneling mechanism efficiently injects electrons into the lasing subband of the single quantum well gain medium. The L-I characteristics of a 200 μm long laser are shown in Fig. 11 with the spectral output shown as an inset. The value of I_{th} is 15 mA and the peak of the emission is at 0.89 μm, noting that the active well is made of $In_{0.1}Ga_{0.9}As$. The modulation response of the laser is shown in Fig. 12, from which $f_{3dB} = 9$ GHz at only 60 mA of injection current. This is a high value considering that the active material is $In_{0.1}Ga_{0.9}As$ and the device has only one lasing quantum well. A direct comparison is not possible since we are not aware of any modulation response data from SQW lasers made with the InGaAs/GaAs/InGaP structure. It compares favorably with our bandwidth of 12.5 GHz mentioned in Sec. 4 and the published data with InGaAs/GaAs/AlGaAs lasers [41-43]. It is expected that further optimization of the structure and the use of $In_{0.35}Ga_{0.65}As$/InGaAsP MQW will lead to much improved performance.

7. MULTIQUANTUM WELL TUNNELING INJECTION LASERS

For a given value of modal gain, the differential gain increases as the number of

quantum wells increases because the carrier density associated with a single quantum well decreases. Improved high frequency performance is achieved in MQW lasers due to the differential gain enhancement [44]. Such a device would also enable the extension of the tunneling concept to a MQW laser. Figure 13(a) shows the schematic heterostructure of the GaAs-based multiple quantum well tunneling injection laser structure grown by MBE. The structure was grown on (100) semi-insulating GaAs substrate. The cladding layers were grown at a substrate temperature of 680 °C. The GaAs and InGaAs quantum wells were grown at 540 °C. It is important to note that the structure is not optimized in terms of number of quantum wells and other parameters.

Figure 13(b) shows the energy band diagram of the MQW tunneling injection laser structure under an applied forward bias, which was obtained by solving the time-independent Schroedinger equation. The dashed lines are the wave functions of the first five states. It can be seen that the wave functions of the first four states are localized in the four quantum wells and the wave function of the fifth state, which is ground state in the cladding region, is localized in the injection layer (inner cladding layer on the n-side). The widths of the quantum wells and the thickness of the GaAs barrier are optimized so that each of the four wave functions in the quantum wells is not localized in an individual well but distributed in the multiple quantum wells and the energies of these four states are very close to each other. Carriers injected into the active region by optical phonon assisted tunneling are uniformly distributed in the multiple quantum wells, resulting in a high differential gain. The calculated tunneling energy is about 72 meV above the lasing subband in the MQW. The exact mechanism of transport is under investigation using time-resolved femtosecond differential transmission spectroscopy.

The 3 μm wide ridge lasers were cleaved to a length of 200 μm and mounted onto copper heatsinks. The lasers were pulse biased with 1 μs pulses having 1% duty cycle. On-wafer measurements were made at heatsink temperatures of 25 °C. The

light-current characteristics of the MQW tunneling injection laser are shown in Fig. 14. The typical threshold current is 20 mA. This high value is due to the non-optimal quality of the AlGaAs cladding layers. The slope efficiency is 0.34 mW/mA per uncoated facet. The peak of the laser emission is at $\sim$ 0.98 μm, which confirms lasing from the MQW region. Fig. 15 shows the modulation frequency response of the MQW tunneling injection laser for increasing drive currents. The measurement was made up to 21 GHz, which is limited by the amplifier and the modulation response is still above 0 dB. The extrapolated -3 dB modulation bandwidth at the highest drive current of 190 mA is $\sim$ 30 GHz, which is much larger than the best modulation bandwidth of 12.5 GHz obtained from the SQW tunneling injection laser. From the plot of damping factor as a function of resonance frequency squared, a K-factor of 0.27 ns was extracted, implying that a maximum -3 dB modulation bandwidth of 33 GHz is achievable if the device is not limited by damping, transport, or device heating. Furthermore, from the plot of resonance frequency versus the square root of the optical output power per facet, a D-factor of 2.3 GHz/mW$^{1/2}$ is obtained. For the purpose of comparison, we also fabricated conventional $In_{0.2}Ga_{0.8}As$/GaAs MQW SCH lasers with four 50 Å wells. There is no tunneling barrier in the structure and the p-side inner cladding layer is 0.1 μm-thick undoped GaAs. The other layers are the same as in Fig. 13(a). The maximum modulation bandwidth of this SCH laser is 16 GHz. It is therefore evident that enhanced high frequency performance can be achieved from the MQW tunneling injection laser.

As stated earlier, our structure is not optimized to achieve the highest possible bandwidth and several parameters can be modified. Higher differential gain can be obtained by increasing the number of quantum wells. Thin inner cladding layers are employed in a laser structure to reduce the influence of carrier transport across the SCH region on modulation performance [42]. Modulation doped MQW lasers are generally used to enhance the differential gain by controlling the quasi-Fermi levels in the band structure [45]. A modulation bandwidth of 37 GHz was reported from p-type

modulation doped InGaAs/GaAs MQW lasers [46]. We believe that the incorporation of these features into the tunneling MQW laser structure will allow the achievement of modulation bandwidth higher than 40 GHz in the TI laser. Furthermore, with the use of the buried-heterostructure design to obtain a true index-guided device with lower threshold current and with proper mounting and heatsinking, GaAs-based MQW tunneling injection lasers have the potential of delivering high output power and demonstrating modulation responses with $f_{-3dB}(max) \sim 60 - 80$ GHz.

8. ULTRA-HIGH BANDWIDTH 0.98 μm TUNNELING INJECTION LASERS

Figure 16 shows the schematic cross section of the MQW TI laser structure. We designed devices with 4-QW and 6-QW gain regions. For the 4-QW structure we have grown two samples, one with an undoped active region and the other with a C-modulation doped active region. The device structure consists of a 0.5 μm-thick n^+-GaAs buffer, a 1μm-thick n-$Al_{0.6}Ga_{0.4}As$ ($n = 5 \times 10^{17}$ cm^{-3}) outer cladding layer, a 0.1 μm-thick undoped GaAs n-side inner cladding or electron injection layer, a 30 Å undoped AlAs tunneling barrier, the active region consisting of four undoped $In_{0.2}Ga_{0.8}As$ quantum wells with different well widths (64, 54, 50 and 48 Å with 70 Å GaAs barriers in between), a 250 Å-thick undoped $Al_{0.1}Ga_{0.9}As$ p-side inner cladding layer, a 1μm-thick p-$Al_{0.6}Ga_{0.4}As$ ($p = 5 \times 10^{17}$ cm^{-3}) outer cladding layer and finally a 0.2 μm-thick p^+-GaAs (3×10^{19} cm^{-3}) top contact layer. The QW barrier is GaAs in the 4-QW structure and $GaAs_{0.92}P_{0.08}$ in the 6-QW structure to compensate the strain in the active region. The structure was grown on (001) GaAs substrate by metal-organic vapor phase epitaxy (MOVPE). The active region was grown at 600°C and the $Al_{0.6}Ga_{0.4}As$ layers were grown at 775°C. Figure 17 shows the energy band diagram and the electron wave functions of the MQW tunneling injection laser structure under a forward bias, which was obtained by solving the time-independent Schrodinger equation. The dashed lines are the wave functions of the first five states. It can be seen that the wave functions of the first four states are localized in the four quantum wells and

the wave function of the fifth state, which is the ground state in the cladding layer, is localized in the injection layer (inner cladding layer on the n-side). The widths of the quantum wells and the thickness of the GaAs barrier are optimized so that each of the four wave functions in the quantum wells is not localized in an individual well but distributed in the multiple quantum wells and the energies of these four states are very close to each other. The coupling of the QWs is important for obtaining a uniform carrier distribution in the MQW structure. The time for electrons to be uniformly distributed in the MQWs is the tunneling time of electrons through the GaAs QW barrier, which is on the order of $(h/(2\pi \Delta E))$ [47]. h is the Planck constant and ΔE is the energy difference between the four states in the MQWs, which is 11 meV in the structure. Since the tunneling energy is designed to be ~ 72 meV above the lasing subband, we believe that carriers thermalize very rapidly by a combination of phonon-assisted tunneling and carrier-carrier scattering. The tunneling time as discussed above is about 2 ps. The details of electron transport and thermalization in these structures are under investigation. Nevertheless, as a result of the fast tunneling and scattering process, compared in time to stimulated emission times, small carrier heating and a high differential gain are expected.

Ridge waveguide single-mode lasers were fabricated with a 3 μm wide stripe in a coplanar ground-signal-ground contact geometry [48]. The p-contact and n-contact metals were Ti/Pt/Au and Ni/Ge/Au/Ti/Au, respectively. The lasers were cleaved to a length of 200 - 800 μm and mounted onto Au-coated copper heatsinks. The facets were uncoated. The measurement was made at room temperature under both CW and pulsed bias conditions. Figure 18 shows the light-current characteristics of the MQW tunneling injection laser with 4-quantum wells. The threshold current is 3 mA for a cavity length of 200 μm. The slope efficiency is 0.33 mW/mA and the differential quantum efficiency is 0.52. From the dependence of the inverse differential quantum efficiency on cavity length, we obtained the internal quantum efficiency $\eta_i = 0.56$ and the internal loss $\alpha_i = 5.2\ cm^{-1}$. The transparency current density, determined from a plot of the threshold current density against inverse cavity length, is only 167 A/cm^2. The peak of the laser emission is

at about 0.98 μm, which confirms lasing from the $In_{0.2}Ga_{0.8}As/GaAs$ MQW region. The emission peak does not shift significantly with C-doping. Single frequency operation has been achieved at currents from 25-30 mA. The characteristic temperature T_o is 178 K, which was obtained in the temperature range between 20° and 80° C.

The small signal modulation characteristics of 200 μm long lasers were measured under CW and pulsed bias conditions with a 50 GHz HP8350B sweep oscillator, a bias-T, a 40 GHz MITEQ amplifier and a 40 GHz New Focus 1011 detector and an HP8562 spectrum analyser. The power of the microwave signal modulating the laser was set between -10 dBm and 0 dBm. The measured response was calibrated for the losses due to cables, connectors, bias network, and DC blocking capacitor. Figure 19(a) shows the modulation frequency response of undoped MQW tunneling injection lasers under CW operation. The maximum modulation bandwidth was obtained at 70 mA. The measurement was made up to 40 GHz, which is limited by the amplifier and the spectrum analyser used in the setup and the modulation response at 40 GHz is about 0 dB. The resonance frequency f_r at 70 mA is 23.5 GHz. The -3dB modulation bandwidth obtained by the curve fitting is 43 GHz. Under pulsed bias condition, the resonance frequency is 26 GHz and the modulation response at 40 GHz is about 6 dB, shown in Figure 19(b). The extrapolated -3dB modulation bandwidth is 48 GHz. This is the highest modulation bandwidth reported to date for any semiconductor laser.

The measured frequency response of the laser was fitted to the standard small signal modulation response to extract modulation parameters, such as the resonance frequency f_r and the damping rate γ as a function of the bias current [49,50]. The resonance frequency is proportional to square root of the output power. From the slope of the linear dependence shown in Figure 20(a) we obtained the value of the figure of merit D = 5.06 GH/$(mW)^{1/2}$ and the differential gain dg/dn = 1.86×10^{-15} cm^2. The damping rate γ varies linearly with f_r squared, and the proportionality constant is the K-factor [20]: $K = 4\pi^2 (\tau_{ph} + \varepsilon/(v_g\, dg/dn))$, where τ_{ph} is the photon life time, ε is the gain compression coefficient , v_g is the group velocity of light and dg/dn

is the differential gain. The maximum possible intrinsic modulation bandwidth is determined solely by the K-factor, $f_{-3dBmax} = 2^{3/2}\pi/K$. From a plot of the damping rate against the resonance frequency squared, shown in Figure20(b), the K-factor was obtained to be 0.116 ns under CW bias condition, representing a maximum intrinsic bandwidth of 76 GHz. Under pulsed bias K is 0.090 ns and $f_{-3dBmax} = 98$ GHz. These are the highest maximum intrinsic modulation bandwidth reported to date for semiconductor lasers. From the values of K-factor and differential gain the gain compression coefficient ε is calculated to be $1.5x10^{-17}$ cm^3 for pulsed bias and $1.7x10^{-17}$ cm^3 for CW operation. The gain compression is minimized in tunneling injection lasers. For the C-doped MQW TI lasers, the threshold current is 12 mA. The internal quantum efficiency η_i and the internal loss α_i are 0.80 and 19 cm^{-1}, respectively. We measured $f_{-3dB} = 30$ GHz at I = 70 mA under CW and $f_{-3dB} = 34$ GHz under pulsed bias. The values of the different modulation parameters obtained by analysing the modulation response data are D = 4.64 GH/$(mW)^{1/2}$, dg/dn = 1.24×10^{-15} cm^2, K = 0.16 ns and $f_{-3dBmax} = 55$ GHz. It is not immediately clear why modulation doping has not enhanced the high speed characteristics of these lasers. Such behaviour has been previously reported[45,51,52].The higher value of α_i in these lasers, possibly arising from free-carrier absorption, may partly account for it, This aspect is under investigation. Nonetheless, the intrinsic modulation bandwidth of the C-doped tunneling injection lasers also surpasses reported results.

Carrier capture times in MQW TI lasers have also been determined from analysis of high frequency electrical impedance measurements. We measured the frequency dependent impedance with an HP8510 Network analyzer at various bias currents. The differential impedance was determined from the measured S-parameters from the relation:

$$Z = Z_o (1 + S_{11})/(1 - S_{11}), \qquad (1)$$

where Zo is the characteristic impedance (50 Ω). The magnitude of the differential impedance is analyzed with the following expressions derived from the rate equations [24]:

$$Z(f) = R_s + R_d T(f) / (1+ 2\pi f \tau_o), \quad (2)$$

Where

$$T(f) = (1 + j2\pi f\tau_1) / (1 + j\, 2\pi f \tau_{eff}) \quad (3)$$

below threshold. R_s is the parasitic series resistance, R_d is the dynamic resistance, and τ_o is the electrical diode time constant which includes the effect of space charge capacitance and capture time. τ_1 is given by $1/\tau_1 = 1/\tau_{eff} + 1/\tau_{esc}$. τ_{eff} and τ_{esc} are the carrier life time in the well and the carrier escape time from the well, respectively. Under conditions of negligible carrier re-emission, where $\tau_{esc} >> \tau_{eff}$, $\tau_1 = \tau_{eff}$ and $T(f) = 1$. The measured impedance is shown in Figure 21 and was fitted to Eq.(2), using τ_o, R_d, and R_s as fitting parameters. The best fit was obtained with $T(f) = 1$, suggesting that τ_{esc} is much larger than τ_{eff}. The carrier life time can be calculated from the slope ($\tan\theta$) of the threshold current density (J_{th}) against inverse cavity length (1/L) [25]:

$$\tan\theta = dJ_{th} / d(1/L) = w\, e\, \ln(1/R_1R_2)/(2\, dg/dn\, \tau_{eff}\, \Gamma), \quad (4)$$

where w is the active layer thickness, dg/dn is the differential gain, Γ is the optical confinement factor, R_1, R_2 are the mirror reflectivities and e is the electron charge. For undoped TI lasers, the differential gain is 1.86×10^{-15} cm^2 and Γ is 0.075. We obtained τ_{eff} is 0.24 ns. Since $\tau_{esc} >> \tau_{eff}$ is applicable for tunneling injection lasers, we may assume that τ_{esc} is of the order of ns. Weisser, et al. [53] determined τ_{eff} and τ_{esc} for an otherwise comparable conventional separate confinement heterostructure $In_{0.35}G_{0.65}As/GaAs$ MQW laser to be 0.3 ns and 0.45 ns, respectively, at threshold. It turns out that in the TI laser the carrier escape time is larger due to the presence of

the tunneling barrier, which prevents carrier from escaping. The extracted value for the capture time is about 1 ps at 50 mA [54], which agrees with the tunneling times obtained from the time resolved DTS measurement. Recent simulations by Grupen and Hess [55], using the Minilase-II simulator have clearly shown that in the tunneling injection laser, the electrons tunneling into the quantum well have low initial energies and therefore minimizes carrier and phonon heating.

As seen in Figure 19, the small-signal modulation response is not damped at the resonance frequency for an injection current of 70 mA, indicating that the high frequency performance of MQW TI-lasers is not damping limited. We believe that the frequency response of these lasers is limited by heating effects. The value of $f_{-3dBmax}$ of 98 GHz in these devices exceeds the predicted gain-compression limited bandwidths of 60 - 70 GHz in high performance quantum well lasers made with this material system [56]. Large bandwidth can only be achieved at the expense of a very high photon density, which would induce facet damage. It is therefore imperative that, to achieve high modulation bandwidths, the laser has to be operated with a lower photon density, the gain compression coefficient has to be reduced and the differential gain has to be enhanced.

9. CONCLUSION

We demonstrate the performance characteristics of tunneling injection lasers, a new class of devices with reduced hot carrier effects. The problem of carrier injection in quantum wells is quantitatively analyzed by calculations and measurements and the tunneling injection mechanism is invoked to alleviate the problem. Higher bandwidths, lower chirp and smaller temperature dependence of the threshold current in 0.98 μm SQW and MQW TI lasers, reduced Auger recombination and temperature dependence of 1.55 μm lasers and a TI laser using the InGaAs/InGaP/GaAs heterostructure are demonstrated. It is therefore demonstrated that the tunneling injection of electrons can be done in a simple manner in any material system and in any device configuration.

PUBLICATIONS

1. "Deep Levels in Si-Implanted and Thermally Annealed GaAs", J.K. Rhee, P. Bhattacharya and R.Y. Koyama, *Journal of Applied Physics,* **53**, 3313 (1982).

2. "Properties of a Tunneling Injection Quantum Well Laser: Recipe for a "Cold" Device with a Large Modulation Bandwidth," H. C. Sun, L. Davis, S. Sethi, J. Singh, and P. Bhattacharya, *IEEE Photonics Technology Letters*, **5(8)**, pp. 870-872, August 1993.

3. "Small-Signal Modulation and Temperature Dependence of the Tunneling Injection Laser", L. Davis, J.C. Sun, H. Yoon, and P.K. Bhattacharya, *Appl. Phys. Lett.,* **64,** pp. 3222-3224, June 13, 1994.

4. "Dynamic Linewidth of Tunneling Injection Laser", H. Yoon, H.C. Sun and P.K. Bhattacharya, *Electronics Letters,* pp. 1675-1676, September 29, 1994.

5. "Carrier Capture and Relaxation in Narrow Quantum Wells", L. Davis, Y.L. Lam, Y.C. Chen, J. Singh, and P. Bhattacharya, *IEEE Jour. of Quan. Elect.,* **30**, pp. 2560-2564, November 11, 1994.

6. "A 'Cold' InP-Based Tunneling Injection Laser with Greatly Reduced Auger Recombination and Temperature Dependence", H. Yoon, A.L. Gutierrez-Aitken, R. Jambunathan, J. Singh and P.K. Bhattacharya, *IEEE Photonics Techn. Lett.,* **7**, 974 (1995).

7. "Tunneling Injection Lasers: A New Class of Lasers with Reduced Hot Carrier Effects", P. Bhattacharya, J. Singh, H. Yoon, X. Zhang, A. Gutierrez-Aitken and Y. Lam, *IEEE Journal of Quantum Electronics,* **32**, pp. 1620-1629, September 9, 1996.

8. GaAs-Based Multiple Quantum Well Tunneling Injection Lasers", X. Zhang, Y. Yuan, A. Gutierrez-Aitken, and P. Bhattacharya, *Appl. Phys. Lett.,* **69**, pp. 2309-2311, October 14, 1996.

9. "0.98 μm Multiquantum Well Tunneling Injection Lasers with Ultra-High Modulation Bandwidths", X. Zhang, A.L. Gutierrez-Aitken, P. Bhattacharya, C. Caneau and R. Bhat, *Electronics Lett.,* **69**, 1715 (1996).

10. "Studies of Carrier Relaxation in Low Dimensional Structures", C.Y. Sung, T.B. Norris, X.K. Zhang, Y.L. Lam, I. Vurgaftman, J. Singh and P.K. Bhattacharya, submitted to *Solid State Electronics.*

11. "0.98 μm Multiple Quantum Well Tunneling Injection Laser with 98 GHz Intrinsic Modulation Bandwidth", X. Zhang, A. Gutierrez-Aitken, D. Klotzkin, and P. Bhattacharya, submitted to *IEEE Jour. of Selected Topics in Quan. Elect. on Semiconductor Lasers",* December 1996.

CONFERENCES

1. "A Tunneling Injection Quantum Well Lasers", H.C. Sun, P. Bhattacharya, J. Singh, L. Davis and S. Sethi, *51st Device Research Conference,* Santa Barbara, June 1993.

2. "Carrier Capture and Relaxation in Narrow Quantum Wells", L. Davis, Y. Lam, Y-C. Chen, S. Sethi, J. Singh and P. Bhattacharya, *Electronic materials Conference,* Santa Barbara, June 1993.

3. "A Tunneling Injection Quantum Well laser: Prospects for a 'Cold' Device with a Large Modulation Bandwidth", H.C. Sun, L. Davis, Y. Lam, S. Sethi, J. Singh and P. Bhattacharya, *20th International Symposium on GaAs and Related Compounds,* Freiburg, Germany, September 1993.

4. "Lasers for Large Modulation Bandwidth and Low Threshold Applications," P. Bhattacharya, L. Davis, H. C. Sun, H. Yoon, S. Sethi, J. Shuttlewood, I. Vurgaftman, and J. Singh, presented at *SPIE's International Symposium,* Los Angeles, CA, January 22-29, 1994.

5. "Carrier Relaxation in Quantum Well, Quantum Wire and Quantum Dot Laser Structures: Consequences for Gain Compression and High-Speed Performance", (INVITED), I Vurgaftman, Y. Lam, P. Bhattacharya and J. Singh, *SPIE (OE/LASE) International Symposium,* Los Angeles, CA, January 1994.

6. "GaAs and InP-Based Monolithically Integrated Transmitters and Photoreceivers (INVITED)", P. Bhattacharya, *IEEE MTT-S International Microwave Symposium,* San Diego, CA, May 1994.

7. "An InP-Based Tunneling Injection Laser with Greatly Reduced Auger Recombination and Temperature Dependence", H. Yoon, P. Bhattacharya, A.L. Gutierrez-Aitken, R. Jambunathan, J. Singh and J.I. Davies, *Indium Phosphide and Related Materials Conference,* Sapporo, Japan, May 1995.

8. "Studies of Carrier Relaxation in Low-Dimensional Structures", C.Y. Sung, T.B. Norris, X. Zhang, Y.L. Lam, I. Vurgaftman, J. Singh and P. Bhattacharya, *Seventh International Conference on Modulated Semiconductor Structures,* Madrid, Spain, July 1995.

9. "Long-Wavelength Lasers and Transmitters: Physics and Technology Roadblocks", P. Bhattacharya, H. Yoon, A. Gutierrez-Aitken, K. Kamath and P. Freeman, presented at the 22nd Int. Symp. Compound Semiconductors, Cheju Island, Korea, August 28-September 2, 1995.

10. "GaAs/InGaAs/AlGaAs (λ=0.98μm) MQW Tunneling Injection Lasers with 84 GHz Intrinsic Modulation Bandwidth Grown by MOVPE", P. Bhattacharya, X. Zhang, Y. Yuan, A. Gutierrez-Aitken, C. Caneau and R. Bhat, *International Conference on Metalorganic Vapor Phase Epitaxy,* Cardiff, UK, June 1996.

11. "MQW Tunneling Injection Lasers (λ=0.98μm) with 84 GHz Intrinsic Modulation Bandwidth", X. Zhang, Y. Yuan, A. Gutierrez-Aitken, P. Bhattacharya, C. Caneau and R. Bhat, *54th Device Research Conference,* Santa Barbara, CA, June 1996.

12. "MQW Tunneling Injection Lasers with K=0.105ns and 84 GHz Intrinsic Modulation Bandwidth", P. Bhattacharya, X. Zhang, Y. Yuan, A. Gutierrez-Aitken, C. Caneau and R. Bhat, *Conference on High Speed Optoelectronics Devices and Systems,* Snowbird, Utah, August 1996.

13. "0.98μm Multiple Quantum Well Tunneling Injection Lasers with 84 GHz Intrinsic Modulation Bandwidth", X. Zhang, Y. Yuan, A. Gutierrez-Aitken and P. Bhattacharya, *Fifteenth International Semiconductor Laser Conference,* Haifa, Israel, October 1996.

PARTICIPATING PERSONNEL

1. H.C. Sun, GSRA
   Ph.D., 1993

2. L. Davis, GSRA
   Ph.D., 1994

3. H. Yoon, GSRA
   Ph.D., 1996

4. Dr. A. Gutierrez-Aitken

5. Dr. X-K. Zhang

INVENTIONS

The Tunneling Injection Laser was invented and developed in this project. It is most effective in reducing hot-carrier related problems in semiconductor lasers (edge-emitting and VCSELs). The tunneling laser has also demonstrated record modulation bandwidths.

BIBLIOGRAPHY

[1] G. P. Agrawal and N. K. Dutta, *Long-Wavelength Semiconductor Lasers.* New York: Van Nostrand Reinhold, 1986.

[2] T. R. Chen, L. E. Eng, B. Zhao, Y. H. Zhuang, and A. Yariv, "Strained single quantum well InGaAs lasers with a threshold current of 0.25 mA," *Appl. Phys. Lett.*, vol. 63, pp. 2621-2623, 1993.

[3] S. Morin, B. Deveaud, F. Clerot, K. Fujiwara and K. Mitsunaga, "Capture of photoexcited carriers in a single quantum well with different confinement structures," *IEEE J. Quantum Electron.*, vol. 27, pp. 1669-1675, 1991.

[4] G. L. Belenky, R. F. Kazarinov, J. Lopata, S. Luryi, T. Tanbun-Ek, and P. A. Garbinski, "Direct measurement of the carrier leakage out of the active region in InGaAsP/InP laser heterostructures," *IEEE Trans. Elec. Dev*, vol. 42, pp. 215-218, 1995.

[5] M. Willatzen, T. Takahasi, and Y. Arakawa, "Nonlinear gain effects due to carrier heating and spectral holeburning in strained-quantum-well lasers," *IEEE Photon. Technol. Lett.*, vol. 4, pp. 682-685, 1992.

[6] W. Rideout, W. F. Sharfin, E. S. Koteles, M. O. Vassell, and B. Elman, "Well-barrier hole burning in quantum well lasers," *IEEE Photon. Technol. Lett.*, vol. 3, pp. 784-786, 1991.

[7] I. Vurgaftman and J. Singh, "Monte Carlo study of electron relaxation in quantum-wire laser structures," *IEEE J. Quantum Electron.*, vol. 30, pp. 2012-2025, 1994.

[8] H. C. Sun, L. Davis, S. Sethi, J. Singh, and P. Bhattacharya, "Properties of a tunneling injection quantum-well laser: recipe for a "cold" device with a large modulation bandwidth," *IEEE Photon. Technol. Lett.*, vol. 5, pp. 870-872, 1993.

[9] M. Yamada and Y. Suematsu, "Analysis of gain suppression in undoped injection lasers," *J. Appl. Phys.*, vol. 52, pp. 2653-2664, 1981.

[10] R. Nagarajan, M. Ishikawa, T. Fukushima, R. S. Geels and J. E. Bowers, "High speed quantum-well lasers and carrier transport effects," *IEEE J. Quantum Electron.*, vol. 28, pp. 1990-2008, 1992.

[11] B. Deveaud, J. Shah, T.C. Damen and W.T. Tsang, "Capture of electrons and holes in quantum wells," *Appl. Phys. Lett.*, vol. 52, pp. 1886-1888, 1988.

[12] R. Kersting, R. Schwedler, K. Wolter, K. Leo and H. Kurz, "Dynamics of carrier transport and carrier capture in $In_{1-x}Ga_xAs/InP$ heterostructures," *Phys. Rev. B*, vol. 46, pp. 1639-1648, 1992.

[13] K. Yokoyama and K. Hess, "Intersubband phonon overlap integrals for AlGaAs/GaAs single-well heterostructures," *Phys. Rev. B*, vol. 31, pp. 6872-6874, 1985.

[14] K. Yokoyama and K. Hess, "Monte Carlo study of electronic transport in $Al_{1-x}Ga_xAs/GaAs$ single-well heterostructures," *Phys. Rev. B*, vol. 33, pp. 5595-5606, 1986.

[15] B. K. Ridley, *Quantum Processes in Semiconductors, 3rd ed.* Oxford University Press, 1993.

[16] L. Davis, Y. L. Lam, Y. C. Chen, J. Singh, and P. K. Bhattacharya, "Carrier capture and relaxation in narrow quantum wells," *IEEE J. Quantum Electron.*, vol. 30, pp. 2560-2564, 1994.

[17] P. W. M. Blom, J. E. M. Haverkort, P. J. van Hall and J. H. Wolter, "Carrier-carrier scattering induced capture in quantum well lasers," *Appl. Phys. Lett.*, vol. 62, pp. 1490-1492, 1993.

[18] P. Lugli and D. K. Ferry, "Electron-electron interaction and high field transport in Si," *Appl. Phys. Lett.*, vol. 46, pp. 594-596, 1985.

[19] C. Jacoboni and P. Lugli, *The Monte Carlo Method for Semiconductor Device Simulation.* New York: Springer-Velag, 1989.

[20] S. M. Goodnick and P. Lugli, "Effect of electron-electron scattering on nonequilibrium transport in quantum-well systems," *Phys. Rev. B*, vol. 37, pp. 2578-2588, 1988.

[21] R. Brunetti, C. Jacoboni, A. Matulionis and V. Dienys, "Effect of interparticle collisions on energy relaxation of carriers in semiconductors," *Physica*, vol. 134B, pp. 369-373, 1985.

[22] C. Y. Sung, T. B. Norris, X. K. Zhang, Y. L. Lam, I. Vurgaftman, J. Singh, and P. K. Bhattacharya, "Studies of carrier relaxation in low dimensional structures," to be published in *Solid State Electron.*, 1996.

[23] C. R. Lutz, Jr., F. Agahi, and K. M. Lau, "Resonant tunneling injection quantum-well lasers," *IEEE Photon. Technol. Lett.*, vol. 7, pp. 596-598, 1995.

[24] F. Girardin, G. Duan, P. Gallion, A. Talneau, and A. Ougazzaden, "Experimental investigation of the relative importance of carrier heating and spectral-hole-burning on nonlinear gain in bulk and strained multi-quantum-well 1.55 μm lasers," *Appl. Phys. Lett.*, vol. 67, pp. 771-773, 1995.

[25] R. Frankenberger and R. Schimpe, "Origin of nonlinear gain saturation in index-guided InGaAsP laser diodes," *Appl. Phys. Lett.*, vol. 60, pp. 2720-2722, 1992.

[26] K. L. Hall, G. Lenz, E. P. Ippen, U. Koren, and G. Raybon, "Carrier heating and spectral hole burning in strained-layer quantum-well laser amplifiers at 1.5 μm," *Appl. Phys. Lett.*, vol. 61, pp. 2512-2514, 1992.

[27] C. K. Sun, H. K. Choi, C. A. Wang, and J. G. Fujimoto, "Femtosecond gain dynamics in InGaAs/AlGaAs strained-layer single-quantum-well diode lasers," *Appl. Phys. Lett.*, vol. 63, pp. 96-98, 1993.

[28] J. Zhou, N. Park, J. W. Dawson, K. J. Vahala, M. A. Newkirk, U. Koren, and B. I. Miller, "Highly nondegenerate four-wave mixing and gain nonlinearity in a strained multiple-quantum-well optical amplifier," *Appl. Phys. Lett.*, vol. 62, pp. 2301-2303, 1993.

[29] M. Willatzen, A. Uskov, J. Mork, H. Olesen, B. Tromborg, and A. P. Jauho, "Nonlinear gain suppression in semiconductor lasers due to carrier heating," *IEEE Photon. Technol. Lett.*, vol. 3, pp. 606-609, 1991

[30] L. Davis, H. C. Sun, H. Yoon, and P. K. Bhattacharya, "Small-signal modulation and temperature dependence of the tunneling injection laser," *Appl. Phys. Lett.*, **64**, pp. 3222-3224, 1994.

[31] S. D. Offsey, W. J. Schaff, L. F. Lester, L. F. Eastman, and S. K. McKernan, "Strained-layer InGaAs-GaAs-AlGaAs lasers grown by molecular beam epitaxy for high-speed modulation," *IEEE J. Quantum Electron.*, vol. 27, pp. 1455-1462, 1991.

[32] N. A. Olsson, N. K. Dutta, and K. Y. Liou, "Dynamic linewidth of amplitude-modulated single-longitudinal-mode semiconductor lasers operating at 1.55 μm wavelength," *Electron. Lett.*, vol 20, pp. 121-122, 1984.

[33] H. Yoon, H. C. Sun, and P. K. Bhattacharya, "Dynamic linewidth of tunneling injection laser," *Electron. Lett.*, vol. 30, pp. 1675-1677, 1994.

[34] H. Yoon, A. L. Gutierrez-Aitken, R. Jambunathan, J. Singh, and P. K. Bhattacharya, "A "cold" InP-based tunneling injection laser with greatly reduced Auger recombination and temperature dependence," *IEEE Photon. Technol. Lett.*, vol. 7, pp. 974-976, 1995.

[35] T. Fukushima, H. Shimizu, K. Nishikata, Y. Hirayama, and M. Irikawa, "Carrier confinement by multiple quantum barriers in 1.55 μm strained GaInAs/AlGaInAs quantum well lasers," *Appl. Phys. Lett.*, vol. 66, pp. 2025-2027, 1995.

[36] C. E. Zah, R. Bhat, B. N. Pathak, F. Favire, W. Lin, M. C. Wang, N. C. Andreadakis, D. M. Hwang, M. A. Koza, T. P. Lee, Z. Wang, D. Darby, D. Flanders, and J. J. Hsieh, "High-performance uncooled 1.3-μm $Al_xGa_yIn_{1-x-y}As$/InP strained-layer quantum-well lasers for subscriber loop applications," *IEEE J. Quantum Electron.*, vol. 30, pp. 511-522, 1994.

[37] Y. K. Sin, H. Horikawa, and T. Kamijoh, "High-power InGaAs-GaAs strained quantum well lasers with InGaP cladding layers on p-type GaAs substrates," *J. Appl. Phys.*, vol. 72, pp. 3212-3214, 1992.

[38] J. M. Olson, R. K. Ahrenkiel, D. J. Dunlavy, B. Keyes, and A. E. Kibber, "Ultralow recombination velocity at $Ga_{0.5}In_{0.5}P$/GaAs heterointerfaces," *Appl. Phys. Lett.*, vol. 55, pp. 1208-1210, 1990.

[39] D. Biswas, N. Debbar, and P. Bhattacharya, "Conduction- and valence-band offsets in GaAs/$Ga_{0.51}In_{0.49}P$ single quantum wells grown by metalorganic chemical vapor deposition," *Appl. Phys. Lett.*, vol. 56, pp. 833-835, 1990.

[40] S. Tiwari and D. J. Frank, "Empirical fit to band discontinuities and barrier heights in III-V alloy systems," *Appl. Phys. Lett.*, vol. 60, pp. 630-632, 1992.

[41] T. Chen, B.Zhao, Y. Yamada, Y. Zhuang, and A. Yariv, "Modulation Bandwidth Enhancement in Single Quantum Well GaAs/AlGaAs Lasers," *Electron. Lett.*, vol. 28, pp. 1989-1991, 1992.

[42] R. Nagarajan, T. Fukushima, M. Ishikawa, J. E. Bowers, R. S. Geels, and L. A. Coldren, "Transport limits in high-speed quantum-well lasers: experiment and theory," *IEEE Photon. Technol. Lett.*, vol. 4, pp. 121-123, 1992.

[43] K. Y. Lau and N. Bar-Chaim, "High-Speed Operation of Single-Quantum-Well Lasers with Large Gain Compression," *IEEE Photon. Technol. Lett.*, vol. 4, pp. 118-120, 1992.

[44] B. Zhao, T. R. Chen, and A. Yariv, "The extra differential gain enhancement in multiple-quantum-well lasers," *IEEE Photon. Technol. Lett.*, vol. 4, pp. 124-126, 1992.

[45] K. Uomi, "Modulation-doped multi-quantum well (MD-MQW) Lasers. I. Theory," *Jpn. J. Appl. Phys.*, vol. 29, pp. 81-87, 1990.

[46] S. Weisser, E. C. Larkins, K. Czotscher, W. Benz, J. Daleiden, J. Fleissner, M. Maier, J. D. Ralston, B. Romero, A. Schonfelder, and J. Rosenzweig, *Proceedings of IEEE/Lasers and Electro-Optics Society Annual Meeting,* vol. 1, pp. 91-92, 1995.

[47] Y. Arakawa, and A. Yariv, "Quantum well lasers - gain, spectra, dynamics," IEEE J. Quantum Electron., vol. QE-22, pp. 1887 - 1899, 1986

[48] S. D. Offsey, W. J. Schaff, P.J. Tasker, and L. F. Eastman, "Optical and microwave performance of GaAs-AlGaAs and strained layer InGaAs-GaAs-AlGaAs graded index separate confinement heterostructure single quantum well lasers," IEEE Photon. Technol. Lett., vol. 2, pp. 9 - 11, 1990

[49] P. A. Morton, T. Tanbun-Ek, R. A. Logan, A. M. Sergent, P. F. sciortino, Jr., and D. L. Coblentz " Frequency response subtraction for simple measurement of intrinsic laser dynamic properties," IEEE Photon. Technol. Lett., vol. 4, pp. 133 - 136, 1992

[50] M. C. Tatham, I. F. Lealman, Colin P. Seltzer, L. D. Westbrook, and D. M. Cooper, "Resonance frequency , damping, and differential gain in 1.5 μm multiple quantum-well lasers," IEEE J. Quantum Electron. vol. QE-28, pp. 408 - 414, 1992

[51] K. Uomi, T. Mishima, and N. Chinone, "Modulation-doped multi-quantum well (MD-MQW) lasers, II. Experiment," Jpn. J. Appl. Phys. vol. 29, pp. 88 - 94, 1990

[52] S. Weisser, J. D. Ralston, E. C. Larkins, I. Esquivias, P. J. Tasker, J. Fleissner and J. Rosenzweig, "Efficient high-speed direct modulation in p-doped $In0_{.35}Ga_{0.65}As/GaAs$ multiquantum well lasers," Electron. Lett., vol. 28, pp. 2141 - 2143, 1992

[53] S. Weisser, I. Esquivias, P. J. Tasker, J.D. Ralston, B. Romero, and J. Rosenzweig, "Impedance characteristics of quantum-well lasers," IEEE Photon. Technol. Lett., vol. 6, pp.1421 - 1423, 1994

[54] D. Klotzkin, X. Zhang, and P. Bhattacharya, "Carrier dynamics in high speed ($f_{-3dB} > 40$ GHz) 0.98 μm multiquantum well tunneling injection lasers determined from electrical impedance measurements," submitted to IEEE Photon. Technol. Lett.

[55] K. Hess and M. Grupen, private communication.

[56] I. Suemune, L. A. Coldren, M. Yamanishi, and Y. Kan, "Extremely wide modulation bandwidth in a low threshold current strained quantum well laser," Appl. Phys. Lett., vol. 53, pp. 1378 - 1380, 1988

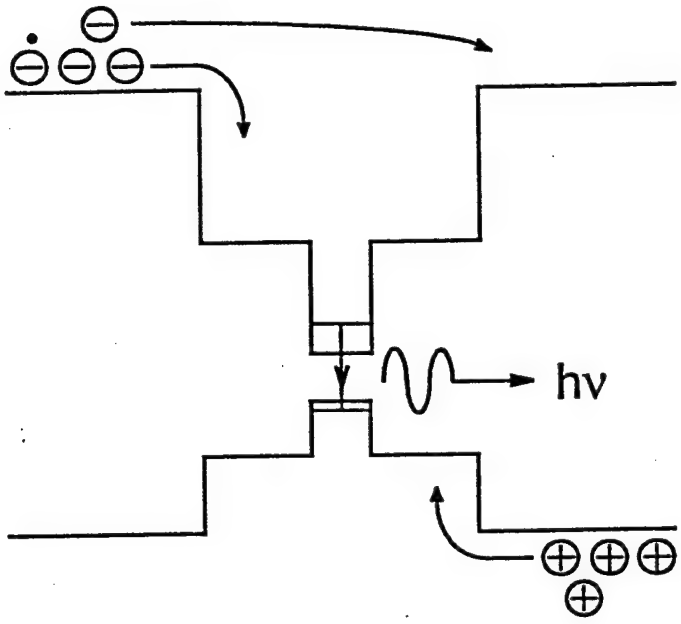

Figure 1

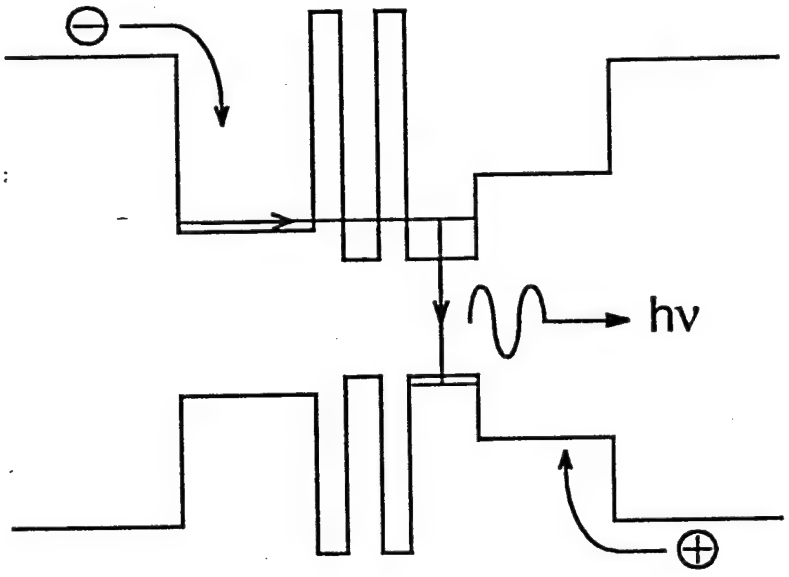

Figure 2

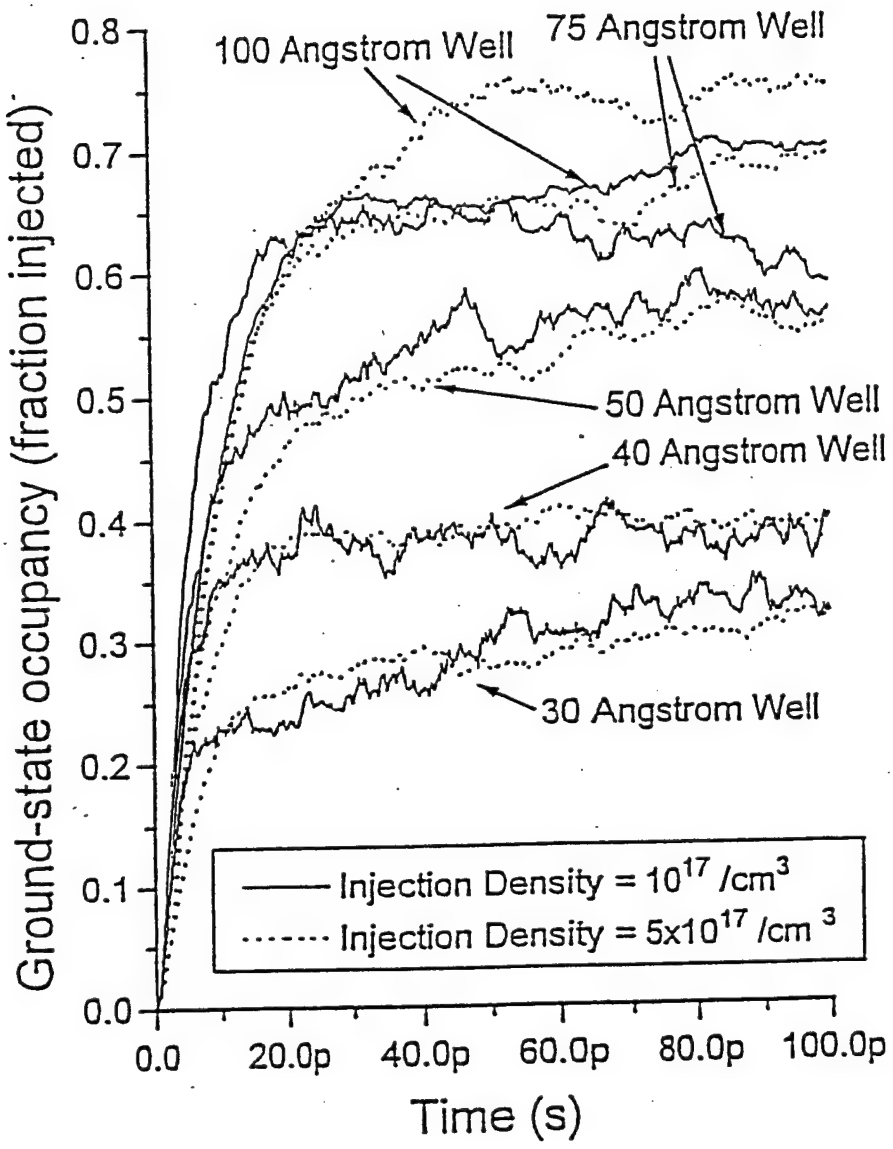
100 Angstrom Well
75 Angstrom Well
50 Angstrom Well
40 Angstrom Well
30 Angstrom Well
Injection Density = 10^17 /cm^3
Injection Density = 5x10^17 /cm^3
Ground-state occupancy (fraction injected)
Time (s)
0.0
0.1
0.2
0.3
0.4
0.5
0.6
0.7
0.8
0.0
20.0p
40.0p
60.0p
80.0p
100.0p

(a)

Figure 3(a)

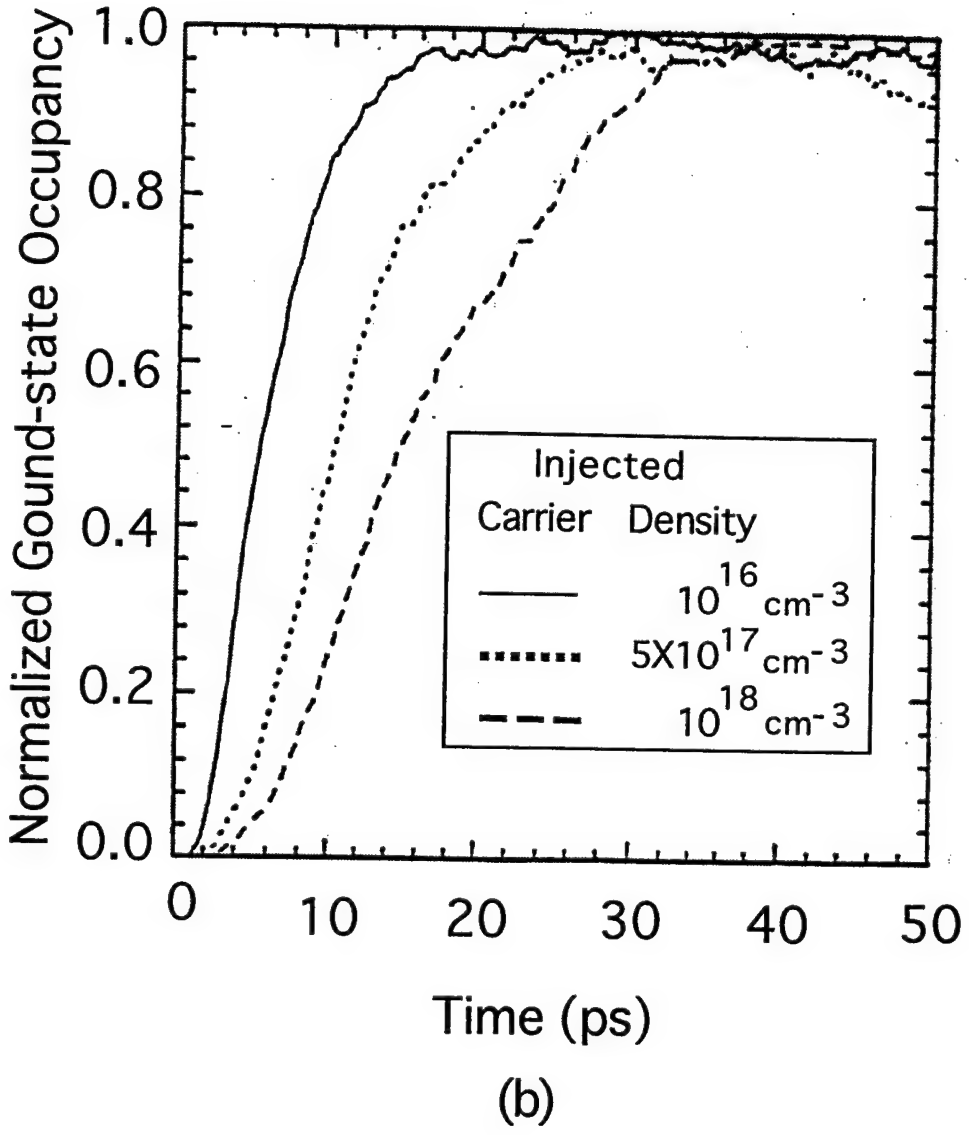
Normalized Gound-state Occupancy
1.0
0.8
0.6
0.4
0.2
0.0
0
10
20
30
40
50
Time (ps)
Injected
Carrier Density
10^16 cm^-3
5X10^17 cm^-3
10^18 cm^-3

(b)

Figure 3(b)

0.1 μm	CONTACT GaAs	$p^+(5\times10^{18}\ cm^{-3})$
1.0 μm	OUTER CLAD $Al_{0.60}Ga_{0.40}As$	$p\ (5\times10^{17}\ cm^{-3})$
0.1 μm	INNER CLAD $Al_{0.30}Ga_{0.70}As$	i
80 Å	ACTIVE WELL $In_{0.10}Ga_{0.90}As$	i
20 Å	Resonant Tunneling Barrier AlAs	i
40 Å	Tunneling Well $In_{0.10}Ga_{0.90}As$	i
20 Å	Tunneling Barrier AlAs	i
0.1 μm	INNER CLAD GaAs	i
1.0 μm	OUTER CLAD $Al_{0.60}Ga_{0.40}As$	$n\ (5\times10^{17}\ cm^{-3})$
0.7 μm	CONTACT GaAs	$n^+(5\times10^{18}\ cm^{-3})$
	S. I. GaAs (100) Substrate	

(a)

0.1 μm	CONTACT $In_{0.53}Ga_{0.47}As$	$p^+(2\times10^{19}\ cm^{-3})$
1.85 μm	OUTER CLAD InP	$p\ (5\times10^{17}\ cm^{-3})$
0.115 μm	INNER CLAD InGaAsP (λ=1.2μm)	i
70 Å	ACTIVE WELL $In_{0.6}Ga_{0.4}As$	i
25 Å	Resonant Tunneling Barrier $In_{0.52}Al_{0.48}As$	i
30 Å	Tunneling Well $In_{0.6}Ga_{0.4}As$	i
25 Å	Tunneling Barrier $In_{0.52}Al_{0.48}As$	i
0.115 μm	INNER CLAD $In_{0.53}Ga_{0.47}As$	i
1.5 μm	OUTER CLAD InP	$n\ (5\times10^{17}\ cm^{-3})$
0.25 μm	CONTACT $In_{0.53}Ga_{0.47}As$	$n^+(5\times10^{18}\ cm^{-3})$
	S.I. InP (100) Substrate	

(b)

Figure 4

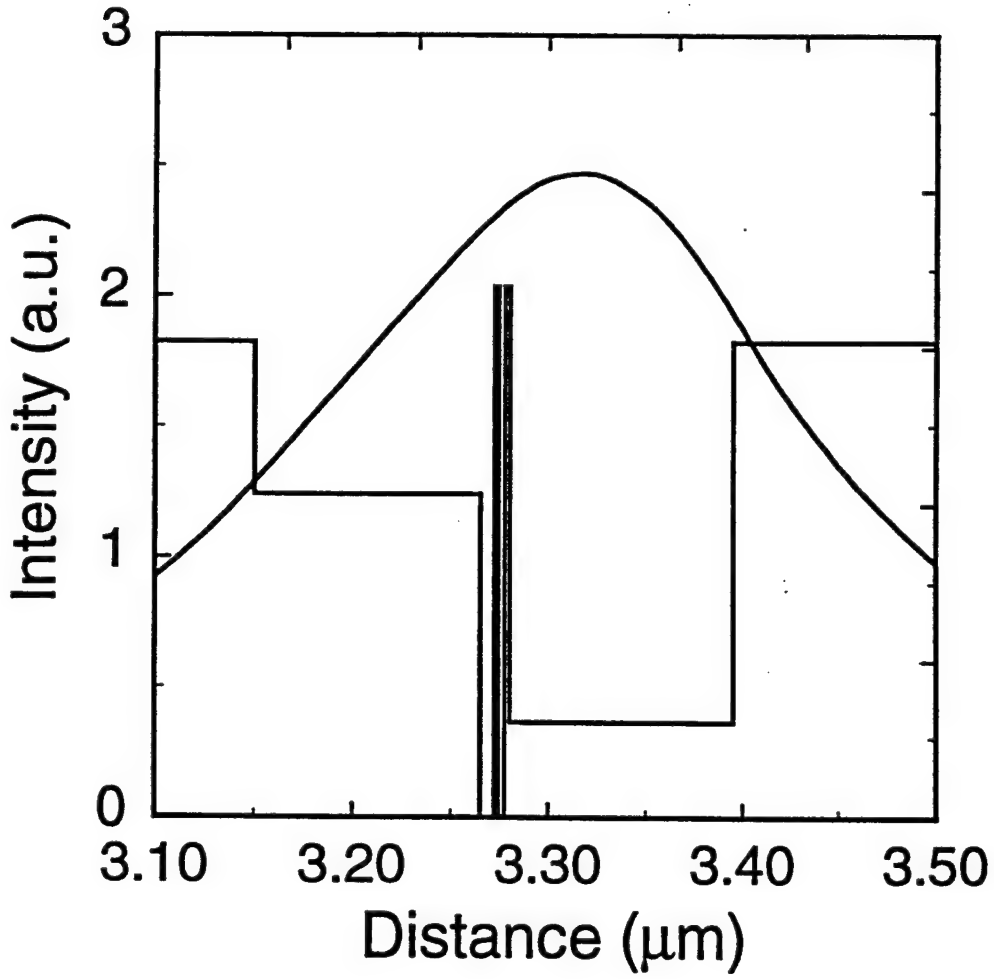

Figure 5

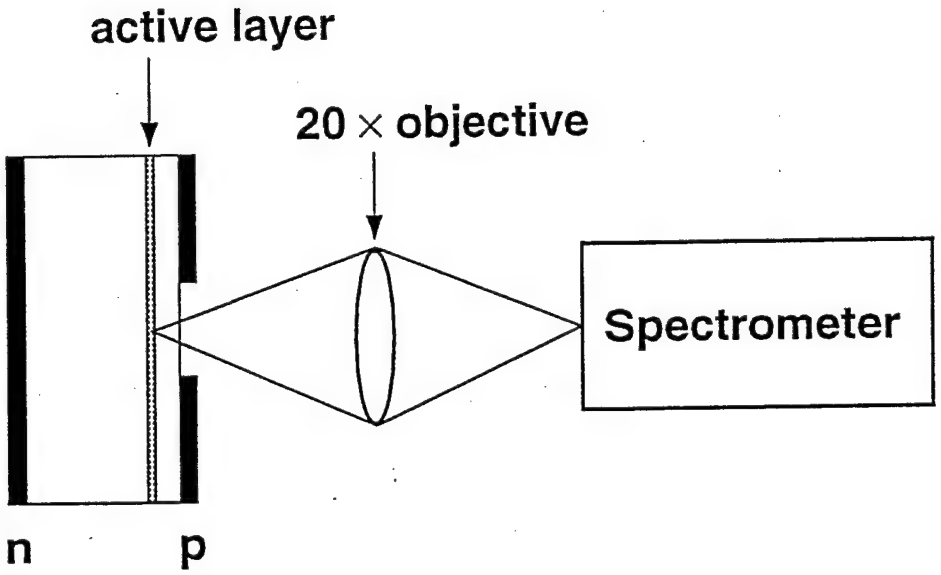

(a)

Figure 6(a)

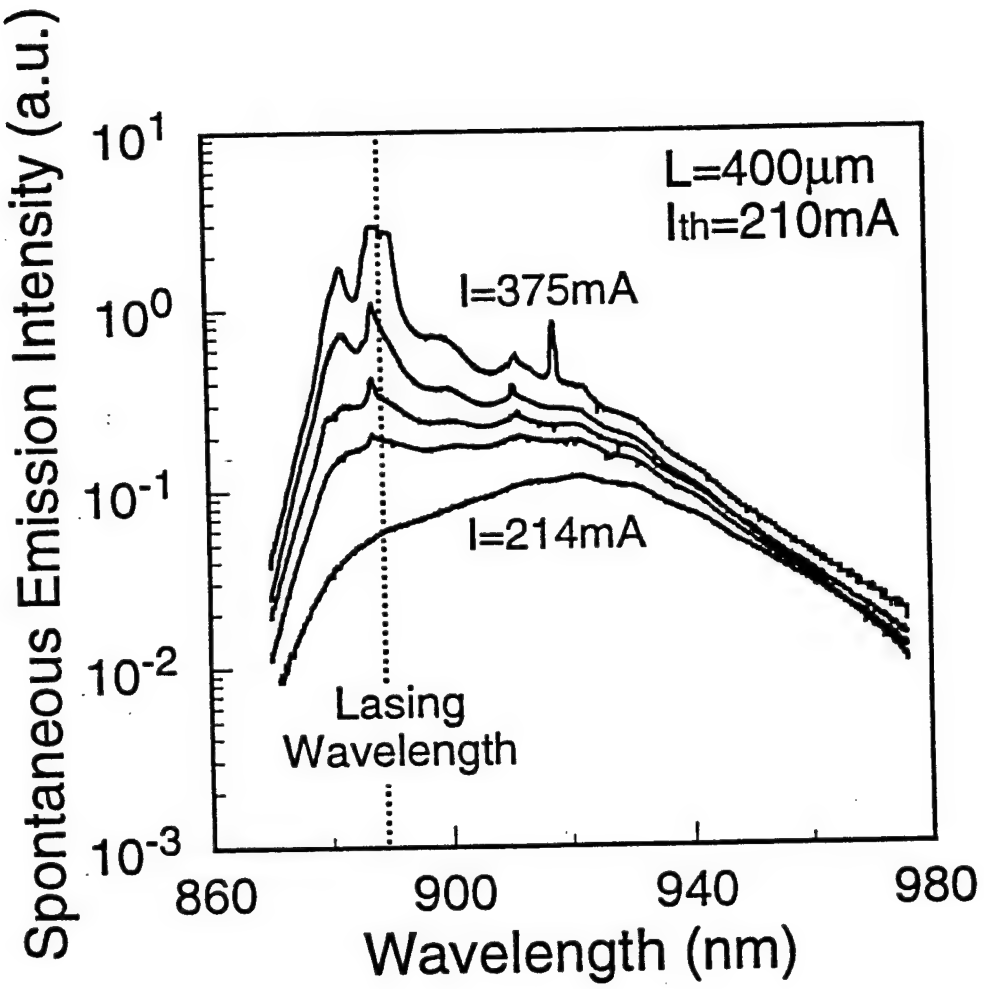
Spontaneous Emission Intensity (a.u.)
10^1
10^0
10^{-1}
10^{-2}
10^{-3}
L=400μm
Ith=210mA
I=375mA
I=214mA
Lasing
Wavelength
860
900
940
980
Wavelength (nm)

(b)

Figure 6(b)

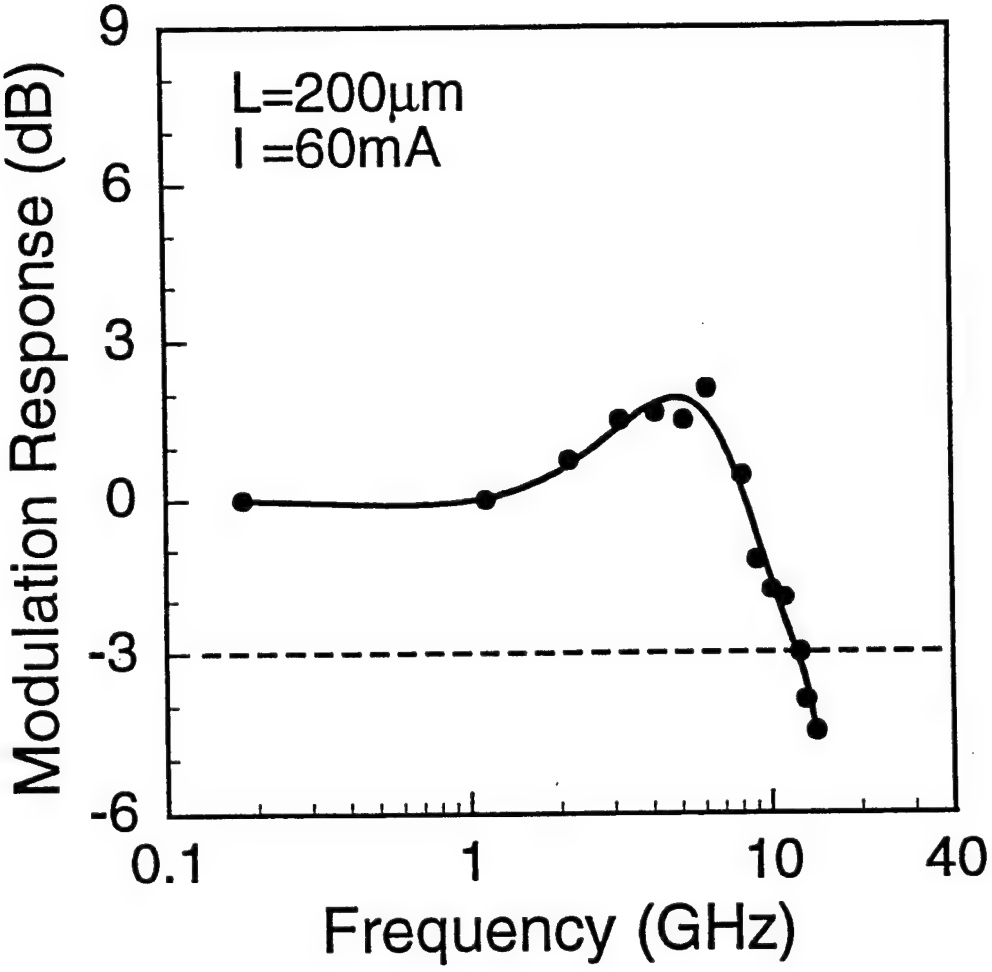
L=200μm
I =60mA
Modulation Response (dB)
9
6
3
0
-3
-6
0.1
1
10
40
Frequency (GHz)

Figure 7

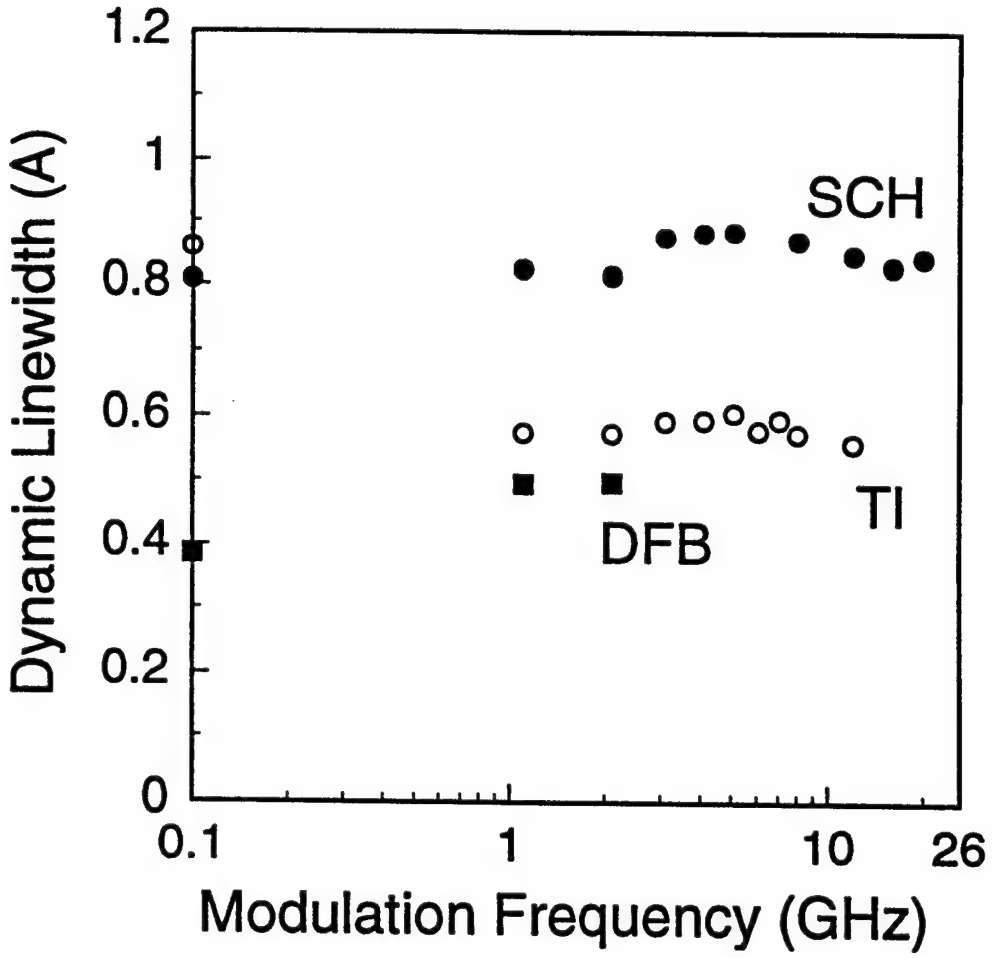
1.2
1
0.8
0.6
0.4
0.2
0
Dynamic Linewidth (A)
SCH
TI
DFB
0.1
1
10
26
Modulation Frequency (GHz)

Figure 8

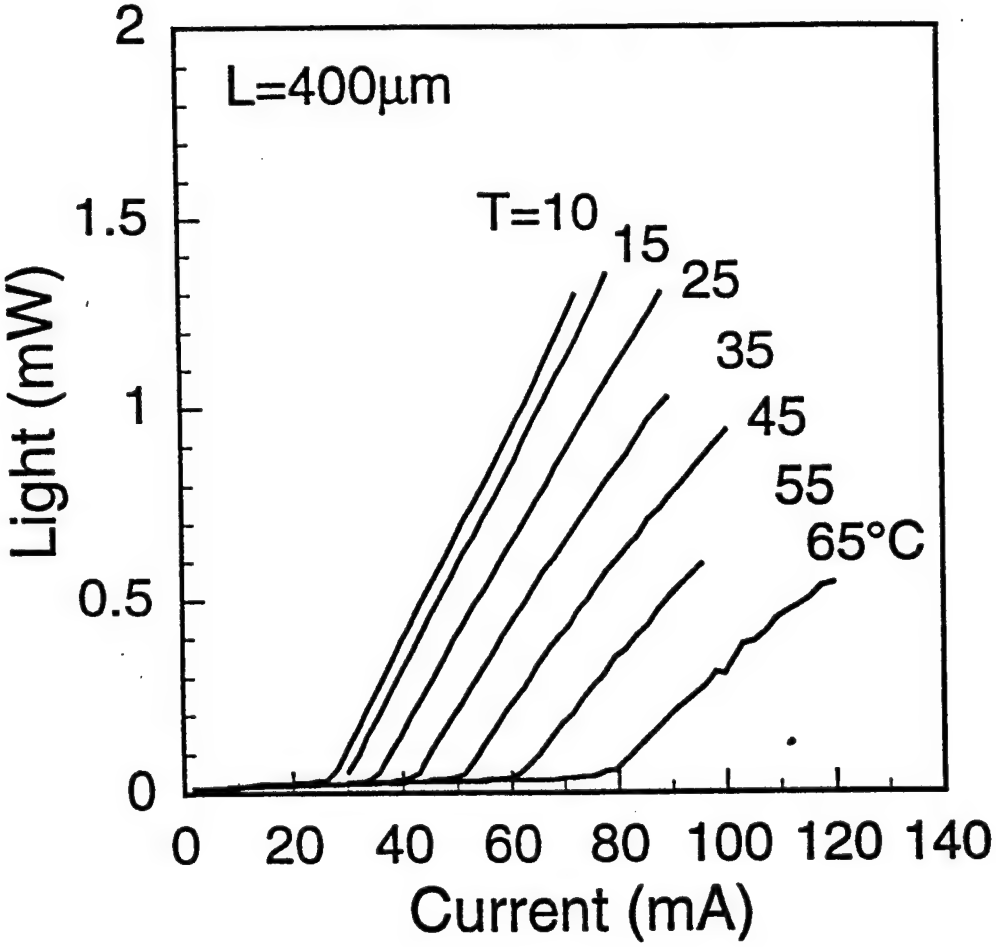
L=400μm
T=10
15
25
35
45
55
65°C
Light (mW)
Current (mA)
0
0.5
1
1.5
2
0
20
40
60
80
100
120
140

Figure 9

0.3 μm	GaAs	$p^+(1\times10^{19}\ cm^{-3})$
1.3 μm	$In_{0.49}Ga_{0.51}P$	$p\ (3\times10^{17}\ cm^{-3})$
0.1 μm	InGaAsP (λ=0.78μm)	i
80 Å	$In_{0.1}Ga_{0.9}As$ Active Well	i
20 Å	$In_{0.49}Ga_{0.51}P$	i
40 Å	$In_{0.1}Ga_{0.9}As$ Tunneling Well	i
20 Å	$In_{0.49}Ga_{0.51}P$	i
0.1 μm	GaAs	i
1.5 μm	$In_{0.49}Ga_{0.51}P$	$n\ (3\times10^{17}\ cm^{-3})$
0.5 μm	GaAs	$n^+(3\times10^{18}\ cm^{-3})$
	S. I. GaAs Substrate	

Figure 10

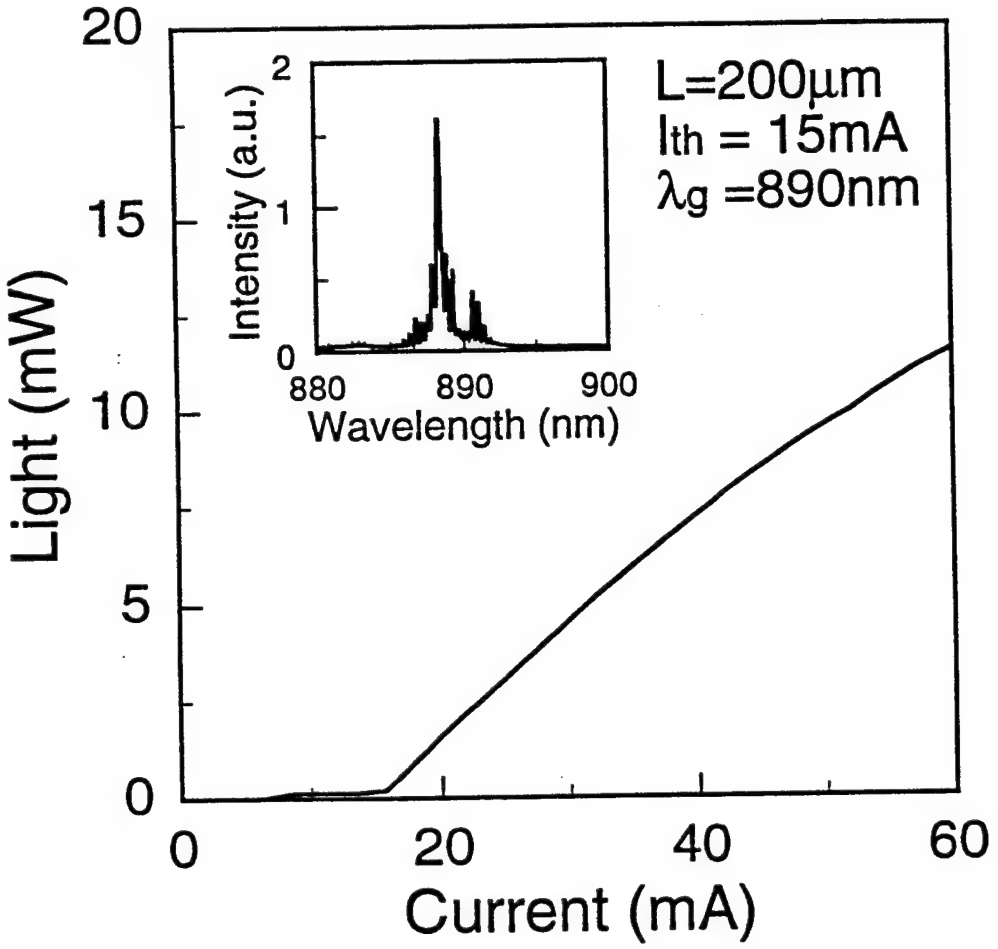
20
15
10
5
0
Light (mW)
0
20
40
60
Current (mA)
L=200μm
Ith = 15mA
λg =890nm
Intensity (a.u.)
2
1
0
880
890
900
Wavelength (nm)

Figure 11

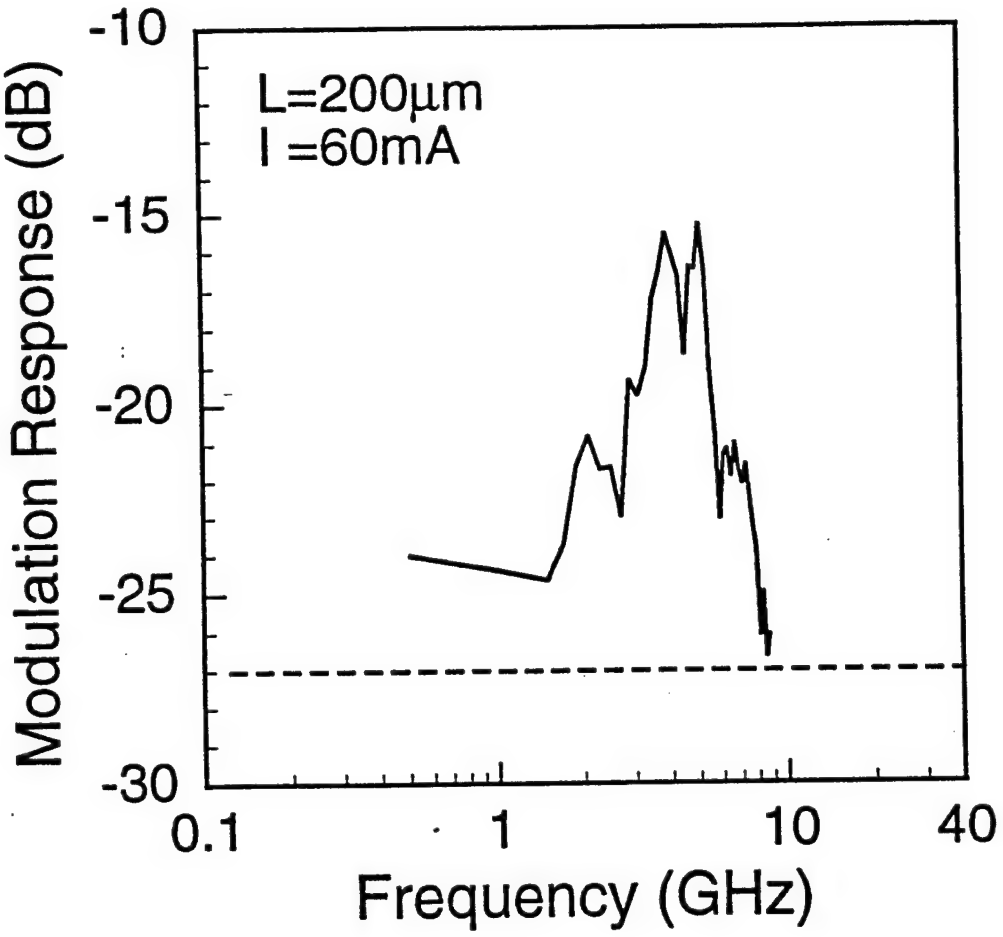
-10
-15
-20
-25
-30
L=200μm
I =60mA
Modulation Response (dB)
0.1
1
10
40
Frequency (GHz)

Figure 12

0.2 μm	GaAs	$p^+(3\times10^{19}\ cm^{-3})$
1.0 μm	$Al_{0.60}Ga_{0.40}As$	$p\ (5\times10^{17}\ cm^{-3})$
0.1 μm	$Al_{0.10}Ga_{0.90}As$	i
48 Å	$In_{0.20}Ga_{0.80}As$	i
70 Å	GaAs	i
50 Å	$In_{0.20}Ga_{0.80}As$	i
70 Å	GaAs	i
54 Å	$In_{0.20}Ga_{0.80}As$	i
70 Å	GaAs	i
64 Å	$In_{0.20}Ga_{0.80}As$	i
30 Å	AlAs	i
0.1 μm	GaAs	i
1.0 μm	$Al_{0.60}Ga_{0.40}As$	$n\ (5\times10^{17}\ cm^{-3})$
0.5 μm	GaAs	$n^+(5\times10^{18}\ cm^{-3})$
	S. I. GaAs (100) Substrate	

(a)

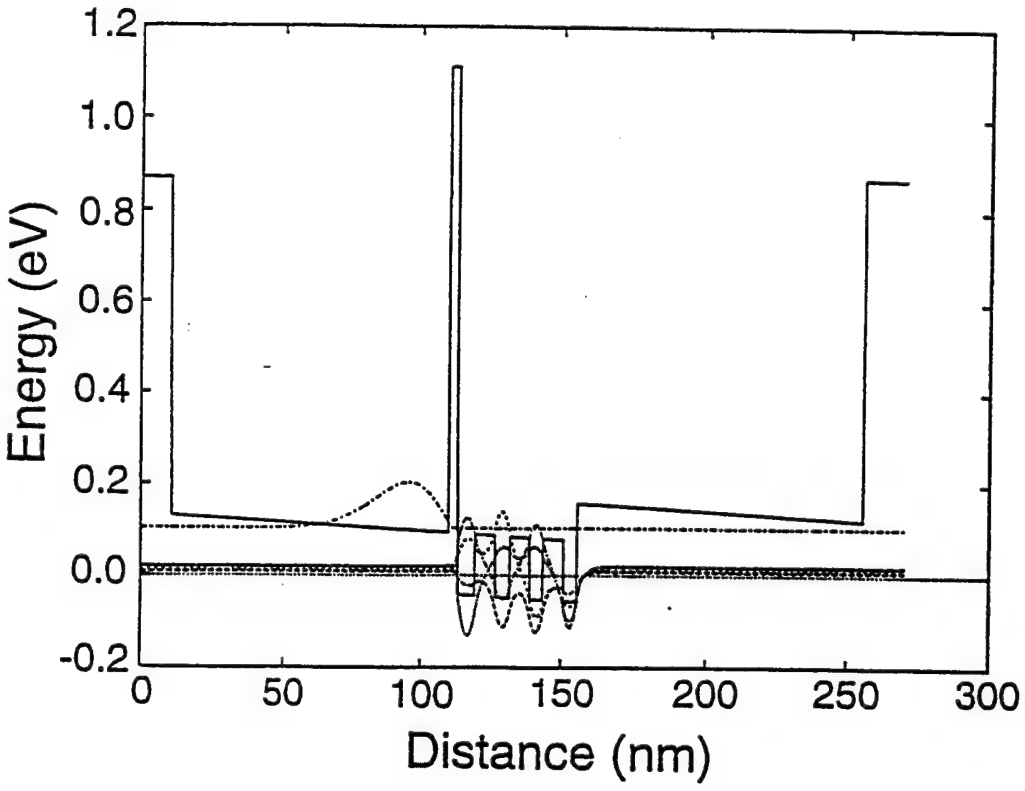

(b)

Figure 13

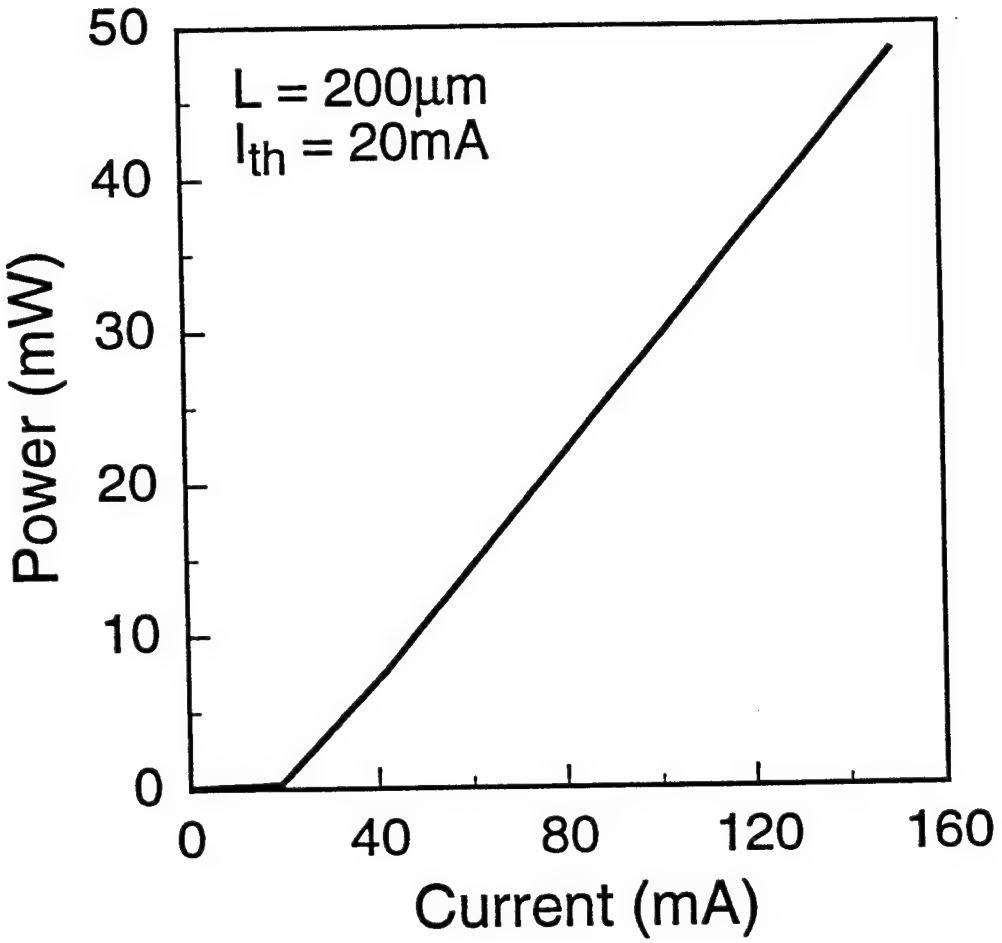
50
40
30
20
10
0
Power (mW)
L = 200μm
I_{th} = 20mA
0
40
80
120
160
Current (mA)

Figure 14

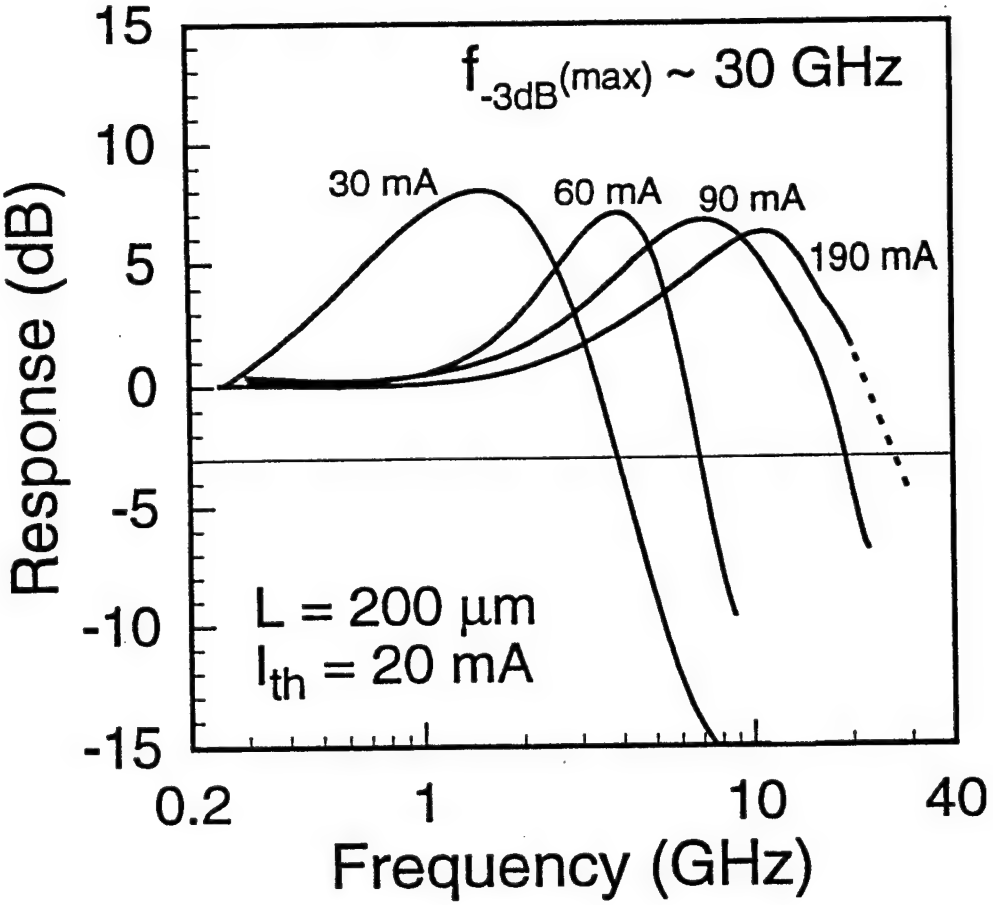
15
10
5
0
-5
-10
-15
Response (dB)
$f_{-3dB(max)}$ ~ 30 GHz
30 mA
60 mA
90 mA
190 mA
L = 200 µm
I_{th} = 20 mA
0.2
1
10
40
Frequency (GHz)

Figure 15

2000Å	p^+	GaAs	$3x10^{19}cm^{-3}$
1μm	p	$Al_{0.6}Ga_{0.4}As$	$5x10^{17}cm^{-3}$
250Å	i	$Al_{0.1}Ga_{0.9}As$	undoped
48Å	i	$In_{0.2}Ga_{0.8}As$	undoped
70Å	i	GaAs	undoped
50Å	i	$In_{0.2}Ga_{0.8}As$	undoped
70Å	i	GaAs	undoped
54Å	i	$In_{0.2}Ga_{0.8}As$	undoped
70Å	i	GaAs	undoped
64Å	i	$In_{0.2}Ga_{0.8}As$	undoped
30Å	i	AlAs	undoped
1000Å	i	GaAs	undoped
1μm	n	$Al_{0.6}Ga_{0.4}As$	$5x10^{17}cm^{-3}$
5000Å	n^+	GaAs	$5x10^{18}cm^{-3}$
	S.I. GaAs Substrate		

Figure 16

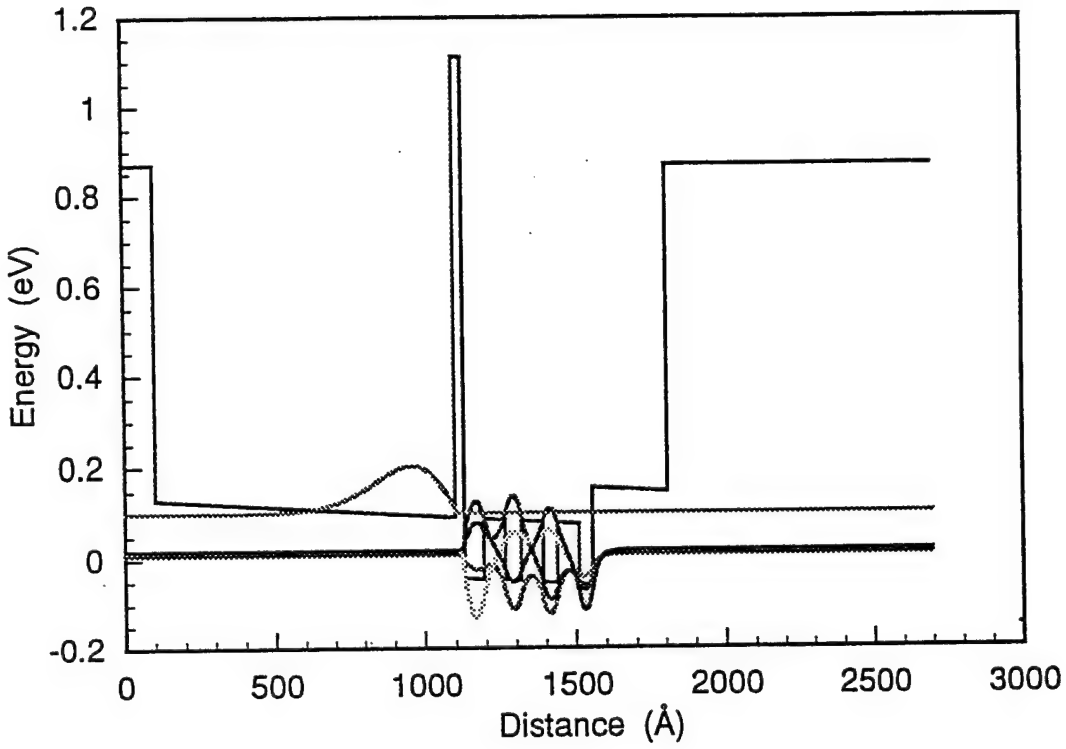
1.2
1
0.8
0.6
0.4
0.2
0
-0.2
Energy (eV)
0
500
1000
1500
2000
2500
3000
Distance (Å)

Figure 17

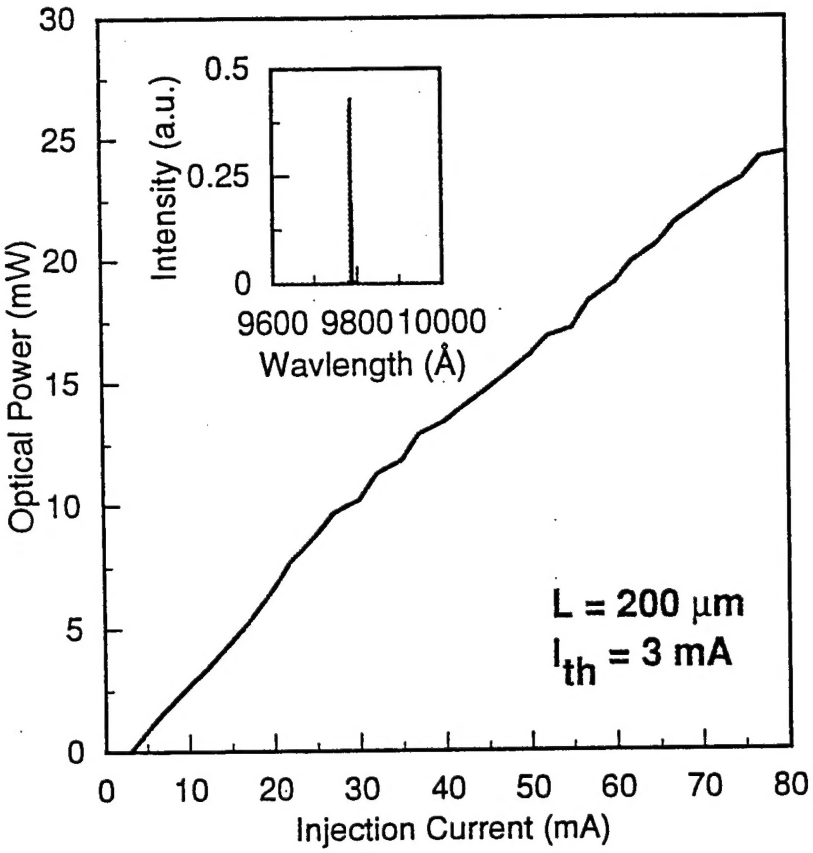
Optical Power (mW)
Injection Current (mA)
Intensity (a.u.)
Wavlength (Å)
L = 200 μm
I_{th} = 3 mA

Figure 18

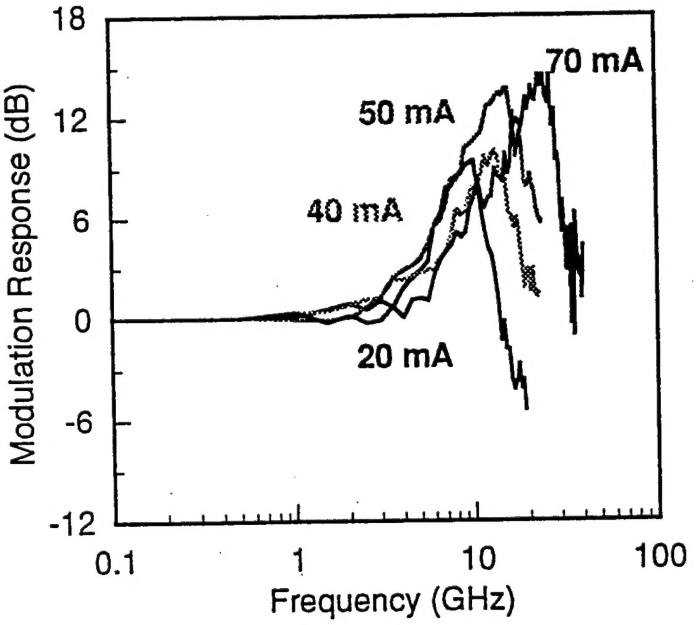
18
12
6
0
-6
-12
Modulation Response (dB)
70 mA
50 mA
40 mA
20 mA
0.1
1
10
100
Frequency (GHz)

(a)

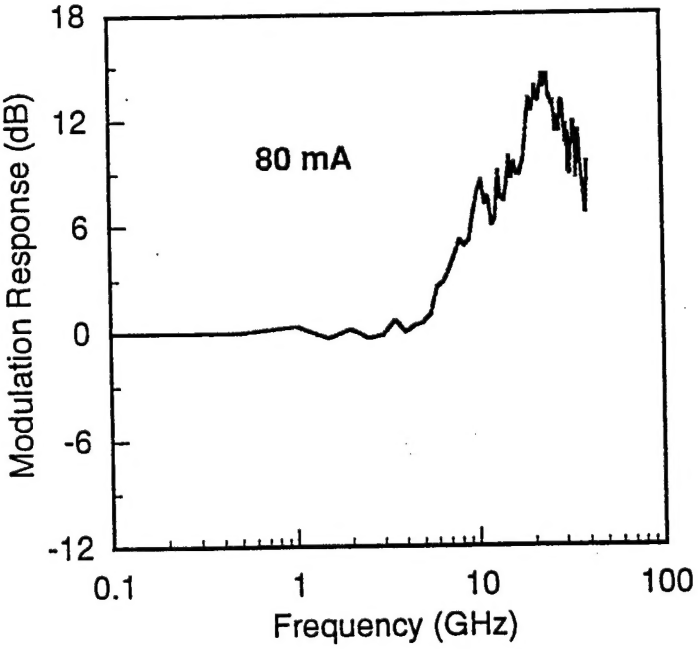
18
12
6
0
-6
-12
Modulation Response (dB)
80 mA
0.1
1
10
100
Frequency (GHz)

(b)

Figure 19

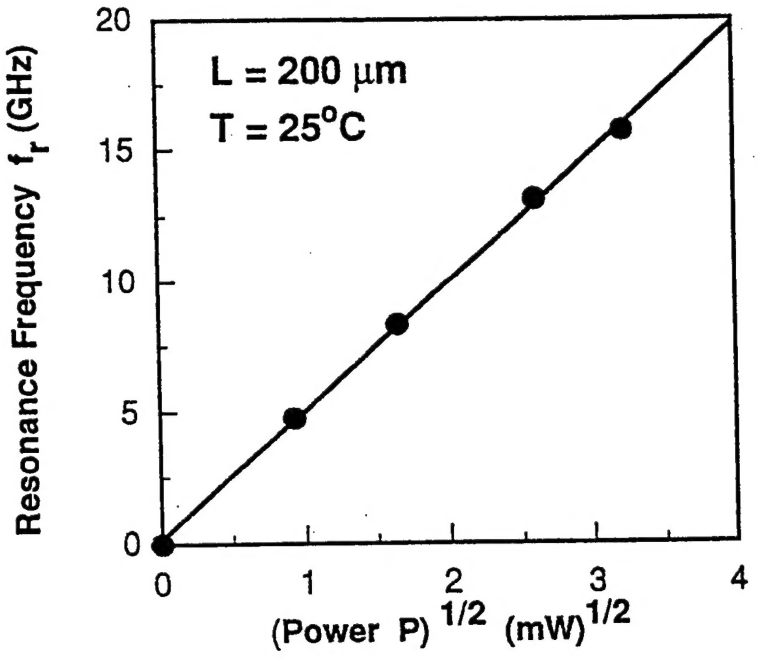
L = 200 μm
T = 25°C
Resonance Frequency f_r (GHz)
(Power P)$^{1/2}$ (mW)$^{1/2}$
0
5
10
15
20
0
1
2
3
4

(a)

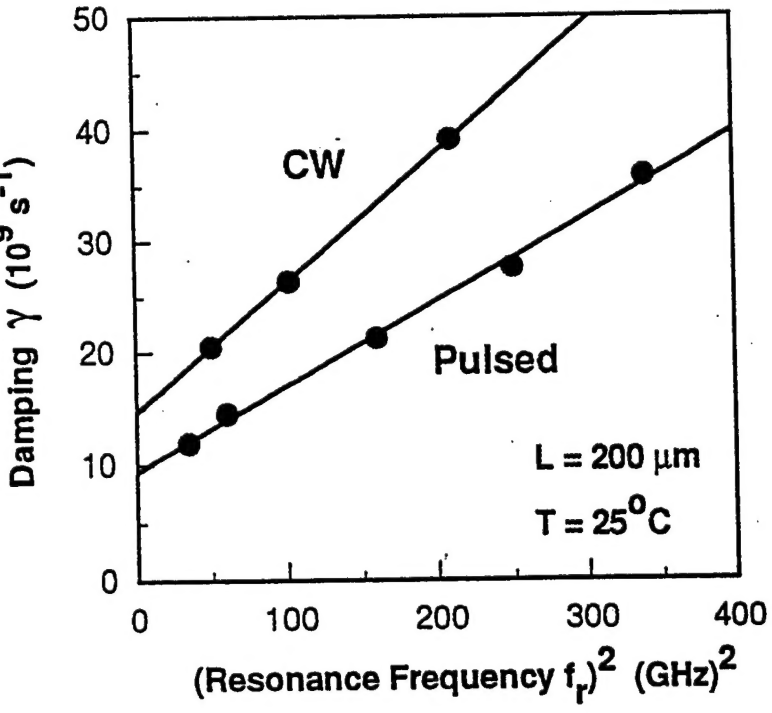
CW
Pulsed
L = 200 μm
T = 25°C
Damping γ (10^9 s^{-1})
(Resonance Frequency f_r)^2 (GHz)^2
0
10
20
30
40
50
0
100
200
300
400

(b)

Figure 20

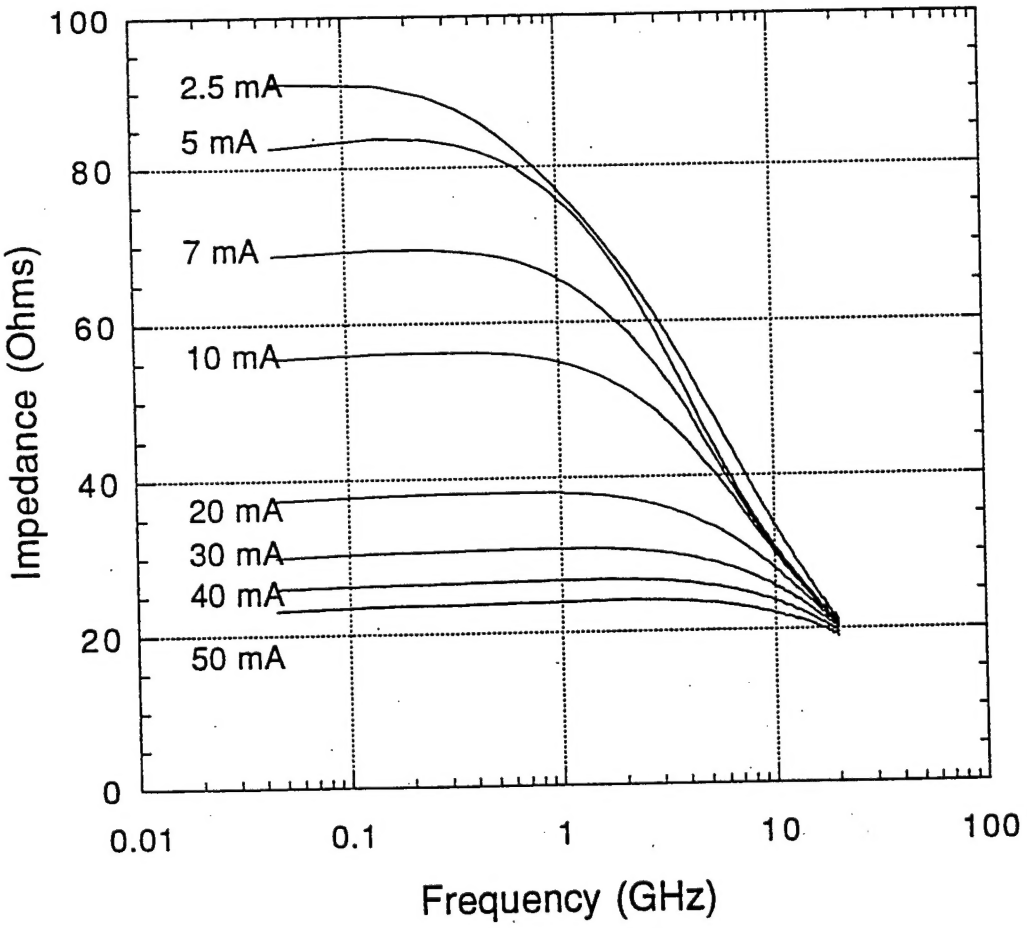
100
80
60
40
20
0
Impedance (Ohms)
2.5 mA
5 mA
7 mA
10 mA
20 mA
30 mA
40 mA
50 mA
0.01
0.1
1
10
100
Frequency (GHz)

Figure 21